Bayesian Operational Modal Analysis of Structures with Tuned Mass Damper

Xinrui Wang[1], Zuo Zhu[2*], Siu-Kui Au[3]

[1]Institute for Risk and Uncertainty and School of Engineering, University of Liverpool, United Kingdom

Email: sgxwan25@student.liverpool.ac.uk

[2]Corresponding author. School of Civil and Environmental Engineering, Nanyang Technological University, Singapore. Email: zuo.zhu@ntu.edu.sg

[3]School of Civil and Environmental Engineering, Nanyang Technological University, Singapore.

Email: ivanau@ntu.edu.sg

Abstract

Tuned mass damper (TMD) is a common strategy to reduce structural vibration in a passive manner without the need for active power. The basic parameters of a TMD include its mass ratio, natural frequency and damping ratio. While these parameters are factory-calibrated before installation, it would be desirable to assess the in-situ properties of the TMD and the 'primary' structure under operational state, e.g., to validate/assess performance and detect detuning over the service life. In this work, a Bayesian approach is developed for identifying the modal parameters of the TMD and primary structure using only the ambient vibration data measured on the primary structure, i.e., 'operational modal analysis'. The likelihood function and theoretical PSD matrix of ambient data are formulated, accounting for primary-secondary structure dynamics with non-classical damping that is not treated in existing Bayesian formulations. An Expectation-Maximisation (EM) algorithm is developed for efficient computation of the most probable value of modal parameters. Analytical expressions are derived so that the 'posterior' (i.e., given data) covariance matrix can be determined accurately and efficiently. The proposed method is verified using synthetic data and applied to field data of a chimney with close modes response attenuated by a TMD.

Keywords:

Ambient vibration test; Tuned mass damper; Operational modal analysis; Close modes; Uncertainty quantification; BAYOMA

1 Introduction

Tuned mass damper (TMD) is a passive control device commonly used for reducing the vibration response of structures, e.g., to improve structural safety and human comfort under various dynamic loadings such as wind, earthquake and traffic [1,2]. It has been widely applied in civil engineering structures such as high-rise buildings [3–7], long-span bridges [8–10], slender towers [11] and industrial chimneys [12,13]. The design of a TMD involves specification of its basic properties, i.e., mass ratio, natural frequency and damping ratio. One classical approach [14] determines the parameters of TMD in some optimal senses under harmonic excitation, neglecting damping of the primary structure, which is often much smaller than that of the TMD. Methods have been developed for designing TMD under different types of loadings and based on different objectives [15,16]. Recent works can be found in [17–20]. To be effective, a TMD needs to be 'tuned', involving a proper choice of its natural frequency and damping for given TMD mass (a constraint) and modal properties of the target structure. The latter is better informed by the in-situ modal properties of the primary structure, which can differ significantly from predictions based on design blueprints. Before installation, the modal properties of a TMD are calibrated against design specifications in the factory. The validation of TMD properties/performance after installation is less trivial and its method/resolution depends on the particular application. Despite the difficulty, the need for in-situ validation is well-substantiated, e.g., from a performance-based perspective of service/product, there can be potential detuning over time arising from changes in TMD or primary structure properties.

'Operational modal analysis' (OMA) aims at identifying the structural modal parameters using 'output-only' ambient vibration data without artificial loadings, which offers an attractive means for determining the in-situ properties of TMD and the primary structure. In the past few decades, OMA has attracted considerable attention for its high implementation economy and feasibility. In OMA, the input excitation is unknown and not measured. It is often assumed to be broadband random. In the context of system identification, or 'inverse' problem, OMA can be approached in a Bayesian or non-Bayesian manner. Non-Bayesian methods [21,22] construct an estimator for modal properties in terms of data, which is often mathematically explicit without the need of numerical optimisation. Among these methods, stochastic subspace identification (SSI) [23–25] and frequency domain decomposition [26] are two popular techniques. The statistical properties such as ensemble mean (related to bias) and ensemble variance (related to identification uncertainty) have been studied, e.g., [27,28] on the uncertainty quantification in SSI methods, [29] on the distribution of Modal Assurance

Criterion (MAC) and [30] on the variance estimation from output-only and input/output subspace-based system identification. Bayesian methods [31–33] view the modal identification as an inference problem where probability is used to assess the plausibility of outcomes given data and model. Bayesian OMA method based on Fast Fourier Transform has been found to be promising because it strictly follows the modelling assumptions and probability logic without the need of artificial averaging or selecting artificial parameters. Working in the frequency domain, it models the unknown input within the resonance band of interest by a stochastic process with constant spectral properties (so only band-limited white) while ignoring other bands with irrelevant information, hence avoiding the modelling error due to potential coloured activities in other bands. For 'globally identifiable' problems [34] such as OMA with typical data length, the distribution of parameters given data and model can be approximated by a Gaussian distribution (see, e.g., Section 8.5 of [33]). The latter is completely characterised by its most probable value and covariance matrix, informing the 'best estimate' and identification uncertainty, respectively.

OMA has been applied to structures with TMD. For example, Weber and Feltrin applied the SSI method to two pedestrian bridges with TMD and observed a significant change of identified damping with seasonal temperature variation [35]. Brownjohn et al. investigated the performance of an aged chimney with TMD based on one-year health-monitoring data, using the SSI method to identify the first two frequencies and damping ratios to assess the vibration reduction efficiency of the TMD [36]. In most existing applications, the properties of TMD are indirectly inferred from the modal properties of the combined primary structure-TMD identified by the OMA method used. Physically 'locking' the TMD (i.e., inhibiting the motion of the TMD relative to the primary structure) may allow one to determine the modal properties of the primary structure [3,37], but not the TMD. Wang and Lin proposed a method to extract the modal frequencies and damping ratios of TMD and primary structure from the combined structure, although the effective TMD modal mass was not identified [38]. Save for exceptions (e.g., [38]), the above applications are based on vibration measurement on the primary structure (not TMD) only, which is an economical option when considering the logistics/interruption required to obtain data from the TMD. Other similar works can be found in, e.g., [39–42].

With the motivation to identify TMD and structural modal parameters explicitly, and to treat the uncertainties in OMA properly, a Bayesian OMA approach is proposed in this work, using ambient vibration data measured at the primary structure only. This necessitates the

formulation of the likelihood function and power spectral density (PSD) matrix of data to account for non-classically damped modal dynamics resulting from the combined structure-TMD system, which is not considered in existing methods. A review of existing structure-TMD dynamics reveals different characteristic behaviours of the frequency response function that depends on TMD parameters (Section 2). This in turn affects the PSD matrix of ambient vibration data (Section 3.2), which dictates the sensitivity of parameters in the modal identification problem and whether they can be uniquely identified. These issues will be investigated analytically (Section 3.3) and the findings will be incorporated into the algorithm for determining the most probable value (MPV), e.g., in the assignment of initial guess. While existing Bayesian OMA theory provides the basic framework for efficient computation, the addition of TMD parameters with different behaviour of PSD matrix necessitates the development of a separate set of algorithms for efficient computation of the MPV (Section 4.1) and 'posterior' (i.e., given data) covariance matrix (Section 4.2). The proposed methodology will be verified using synthetic data of a multi-storey building under various TMD configurations (Section 5). It will also be applied to field data from a chimney with close modes response attenuated by TMD (Section 6).

2 Single-degree-of-freedom structure with TMD

The dynamics of a single-degree-of-freedom (SDOF) primary structure equipped with a TMD is reviewed in this section; further details may be referred to [14–16]. The presentation here provides the background to the basic behaviour of dynamic amplification of acceleration response and hence the power spectrum of measured vibration data, which reveals the nature of the OMA problem and identifiability. The general case of a multi-degree-of-freedom (MDOF) primary structure equipped with TMD is considered later in Section 3, where the PSD x matrix of data and likelihood function will be derived. When there is no confusion, for conciseness, the primary structure is simply referred as 'structure'.

Consider a SDOF structure with displacement x, mass m, stiffness k and damping c subjected to force (per unit structural mass) w; see Figure 1. It is installed with a TMD with displacement υ (relative to the primary structure), mass m_d, stiffness k_d and damping c_d.

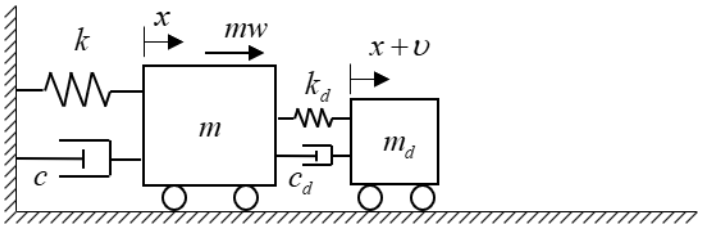

Figure 1 Schematic diagram of a SDOF structure with a TMD.

The equations of motion of the structure and the TMD are respectively given by (omitting dependence on time t)

$$m\ddot{x} + c\dot{x} + kx - (c_d\dot{\upsilon} + k_d\upsilon) = mw \tag{1}$$

$$m_d\ddot{\upsilon} + c_d\dot{\upsilon} + k_d\upsilon = -m_d\ddot{x} \tag{2}$$

In terms of natural frequencies and damping ratios, these can be written as

$$\ddot{x} + 2\zeta_1\omega_1\dot{x} + \omega_1^2 x - \mu(2\zeta_d\omega_d\dot{\upsilon} + \omega_d^2\upsilon) = w \tag{3}$$

$$\ddot{\upsilon} + 2\zeta_d\omega_d\dot{\upsilon} + \omega_d^2\upsilon = -\ddot{x} \tag{4}$$

where $\omega_1 = \sqrt{k/m}$ (rad/sec) is the natural frequency and ζ_1 is the damping ratio of the primary structure; $\omega_d = \sqrt{k_d/m_d}$ (rad/sec) and ζ_d are respectively the natural frequency and damping ratio of the TMD; $\mu = m_d/m$ is the mass ratio. The frequency response function (FRF) between the excitation w and acceleration response $\ddot{x}$ can be derived by considering the Fourier Transform (FT) of the governing equations and eliminating the FT of υ (and its derivatives). Specifically, let $\mathcal{F}_{\ddot{\upsilon}}(\omega)$ denote the FT of $\ddot{\upsilon}$ at frequency ω; a similar notation applies to other quantities. Taking the FT of (4), using $\mathcal{F}_{\dot{\upsilon}} = (\mathbf{i}\omega)^{-1}\mathcal{F}_{\ddot{\upsilon}}$, $\mathcal{F}_{\upsilon} = -\omega^{-2}\mathcal{F}_{\ddot{\upsilon}}$, and rearranging gives ($\mathbf{i}^2 = -1$)

$$\mathcal{F}_{\ddot{\upsilon}} = -h_d\mathcal{F}_{\ddot{x}} \tag{5}$$

where

$$h_d = [1 - \beta_d^2 - 2\zeta_d\beta_d\mathbf{i}]^{-1} \qquad \beta_d = \frac{\omega_d}{\omega} \tag{6}$$

is the FRF (except for a sign) between the acceleration response of the primary structure and that of TMD. From (4) again, $-(2\zeta_d\omega_d\dot{\upsilon} + \omega_d^2\upsilon) = \ddot{x} + \ddot{\upsilon}$. Substituting into (3) and taking FT, using $\mathcal{F}_{\ddot{\upsilon}} = -h_d\mathcal{F}_{\ddot{x}}$ in (5), collecting terms and rearranging gives $\mathcal{F}_{\ddot{x}} = g\mathcal{F}_w$, where

$$g = [1-\beta^2 + \mu(1-h_d) - 2\zeta_1\beta\,\mathbf{i}]^{-1} \qquad \beta = \frac{\omega_1}{\omega} \tag{7}$$

is the FRF between the input force and acceleration of the primary structure. As expected, g reduces to the FRF in the nominal case (i.e., without TMD) when $\mu = 0$. Substituting h_d in (6) into (7) and simplifying gives an expression explicitly in terms of all parameters:

$$g = \frac{1-\alpha^2\beta^2 - 2\zeta_d\alpha\beta\,\mathbf{i}}{[(1+\mu-\beta^2)(1-\alpha^2\beta^2) - \mu - 4\zeta_1\zeta_d\alpha\beta^2] - [2\zeta_1\beta(1-\alpha^2\beta^2) + 2\zeta_d\alpha\beta(1+\mu-\beta^2)]\,\mathbf{i}} \tag{8}$$

where $\alpha = \omega_d/\omega_1$ is the 'TMD frequency ratio'. The dynamic amplification factor between the excitation and acceleration response of the primary structure is given by

$$D = |g|^2 = \frac{(1-\alpha^2\beta^2)^2 + (2\zeta_d\alpha\beta)^2}{[(1+\mu-\beta^2)(1-\alpha^2\beta^2) - \mu - 4\zeta_1\zeta_d\alpha\beta^2]^2 + [2\zeta_1\beta(1-\alpha^2\beta^2) + 2\zeta_d\alpha\beta(1+\mu-\beta^2)]^2} \tag{9}$$

As a check, D reduces to the dynamic amplification factor in the nominal case (i.e., without TMD) when $\mu = 0$ (zero TMD mass) or $\alpha = 0$ (zero TMD stiffness); or when $\alpha = \infty$ or $\zeta_d = \infty$ (in either case, TMD 'sticking' to the primary structure, hence losing its DOF), except that the term $1-\beta^2$ becomes $1+\mu-\beta^2$ reflecting an additional mass due to the TMD.

2.1 Frequency response characteristics

Vibration data collected from a structure tuned by TMD can have frequency characteristics that look abnormal compared to that from a lightly damped structure without TMD. Figure 2 shows the dynamic amplification D in (9) for different values of ζ_d, covering three cases of different nature. For illustration purpose, we have assumed $f_1 = \omega_1/2\pi = 1$ Hz, $\zeta_1 = 1\%$, $\mu = 2\%$ and $\alpha = 0.96$. In this case, the optimal value of ζ_d based on the classical approach is about 8%; see (31) in Section 5 later and also Chapter 3 of [14]. Several features are worth noting. When ζ_d is smaller than the optimal value, there are two peaks near the natural frequencies of the combined structure-TMD system, i.e., about 0.9 Hz and 1.05 Hz in this case. The trough is near the TMD frequency $f_d = f_1\alpha$, i.e., about 0.96 Hz in this case. As ζ_d increases, the two peaks become closer and their values decrease, while the value of trough increases. When ζ_d increases roughly beyond the optimal value, the two peaks degenerate into a single peak whose

value tends to increase with ζ_d. These observations are intuitively related to the action of the TMD. When ζ_d is too small, the TMD (being an additional DOF) adds one sharp peak to the amplification factor, but it is not effective in reducing response. At the other extreme, when ζ_d is too large, the TMD 'sticks' to the structure without effectively dissipating energy by resonance, and so the dynamic amplification behaves like the ordinary one (i.e., without TMD) with a slightly increased structural mass due to TMD. When ζ_d is near the optimal value, the two peaks tend to even out in values, which in fact offers a simple criterion to reduce response in a robust manner for a range of neighbouring frequencies. To supplement, when $\zeta_d = 0$, the two peaks tend to infinity and they are located exactly at the natural frequencies of the combined structure; the trough is located exactly at $f_d = f_1\alpha$. See Appendix A for a further discussion on the dynamic characteristics of the undamped structure (i.e., $\zeta_1 = 0$) with a TMD, which also forms the basis of the choice of initial guess in modal identification (See later in Section 4.1).

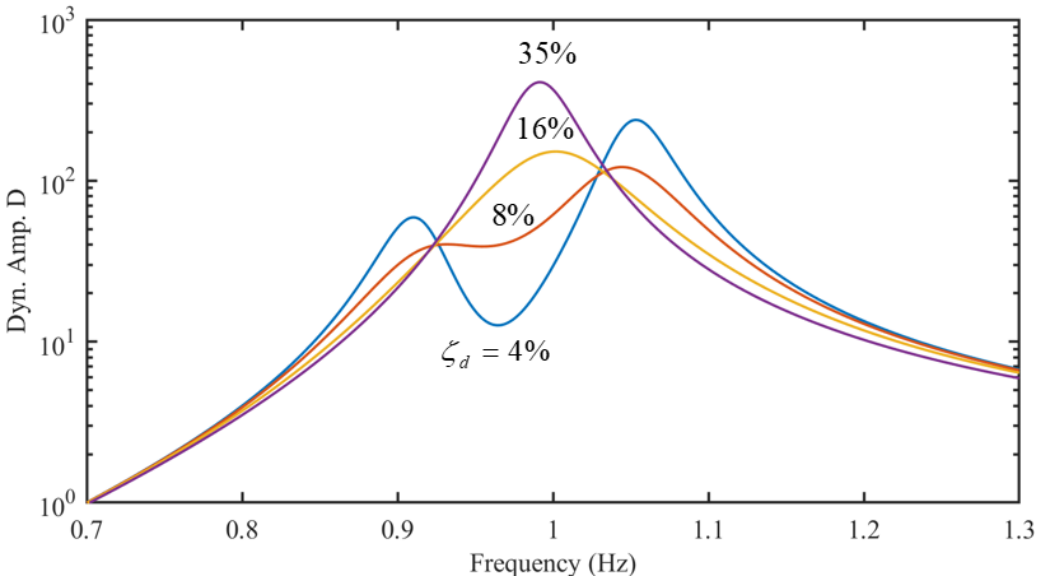

Figure 2 Dynamic amplification D in (9) for different values of TMD damping ratio ζ_d; $f_1 = 1$ Hz, $\zeta_1 = 1\%$, $\mu = 2\%$, $\alpha = 0.96$; the classical optimal design is near $\alpha = 0.98$ and $\zeta_d = 8\%$.

Figure 2 and the associated behaviours described above have implications on the modal information that can be inferred from vibration data and how the results should be interpreted. In particular, for cases such as $\zeta_d = 16\%$ and 35% in Figure 2, the dynamic amplification has

only a single peak and its variation is similar to that in the ordinary case (i.e., without TMD). Assuming broadband excitation, the same applies to the power spectrum of data. For these cases, TMD actions may become unnoticed and one is likely to identify the modal properties as in the ordinary case without TMD in mind. In fact, for sufficiently large ζ_d, modal parameters such as mass ratio and TMD damping ratio could be challenging to identify since the data may not carry enough information to distinguish the characteristics of the TMD from the combined system.

3 Bayesian OMA formulation for MDOF structure with TMD

In this section, a Bayesian formulation is proposed for identifying the modal properties of a (primary) structure equipped with a TMD. The (primary) structure is assumed to be classically damped, although the combined structure-TMD system is non-classically damped. The TMD is modelled by a SDOF viscously damped spring-mass-damper attached to a particular DOF with a (fix-base) frequency near a particular mode of the structure. Modal identification is based on ambient vibration data collected from the primary structure only, which is a typical scenario in applications that does not involve logistics/interruption of TMD operations.

Applying Bayesian concepts/assumptions (Section 3.1) to the problem leads to the same form of the likelihood function in (11) as in conventional Bayesian OMA (BAYOMA) formulations [33]. The differences lie in the PSD matrix of data (see (18)) and the set of modal parameters to be identified. The key in deriving the analytical expression for the PSD matrix lies in the FRF between the modal excitations and response data. Existing techniques of TMD dynamics (which can be seen as an extension of Section 2) are applied to derive the FRF (Section 3.2). Special attention should be made to the mathematical structure of the FRF, however, because it generally comprises too many parameters (e.g., related to the orientation of TMD) that cannot be identified from measured data collected only at the primary structure. In view of this, a parameter scheme is proposed so that the parameters can be uniquely identified, i.e., the Bayesian inference problem is globally identifiable [34]. Identifiability issues are discussed in Section 3.3.

3.1 Bayesian inference

Let $\{\hat{\ddot{\mathbf{x}}}_j\}_{j=0}^{N-1}$ $(n\times 1)$ be the time-domain acceleration data measured at n DOFs of the primary structure at time interval Δt (sec); N is the number of samples per data channel. Its (one-sided)

scaled Fast Fourier Transform (FFT) at frequency $\mathrm{f}_k = k/N\Delta t$ (Hz) is defined as $\mathcal{F}_k = \sqrt{2\Delta t/N}\sum_{j=0}^{N-1}\hat{\ddot{\mathbf{x}}}_j e^{-2\pi \mathbf{i} jk/N}$, where $\mathbf{i}^2 = -1$. Following a Bayesian approach, the identification result for modal parameters is encapsulated in the 'posterior' probability density function (PDF). Assuming a uniform prior distribution for the modal parameters, the posterior PDF is proportional to the 'likelihood function'. Let $\boldsymbol{\theta}$ denote the set of parameters to be identified and $\{\mathcal{F}_k\}$ be the scaled FFT within a selected frequency band covering the modes of interest. Then the posterior PDF is given by

$$p(\boldsymbol{\theta}\,|\,\{\mathcal{F}_k\}) \propto p(\{\mathcal{F}_k\}\,|\,\boldsymbol{\theta}) = e^{-L(\boldsymbol{\theta})} \tag{10}$$

where

$$L(\boldsymbol{\theta}) = nN_f \ln \pi + \Sigma \ln |\,\mathbf{E}_k(\boldsymbol{\theta})\,| + \Sigma \mathcal{F}_k^* \mathbf{E}_k(\boldsymbol{\theta})^{-1} \mathcal{F}_k \tag{11}$$

is the 'negative log-likelihood function' (NLLF) that is often used for analysis and computation; the sum is over f_k in the selected band with N_f FFT points; and $\mathbf{E}_k = E[\mathcal{F}_k \mathcal{F}_k^*]$ is the theoretical PSD matrix of measured vibration data that depends on modal parameters $\boldsymbol{\theta}$. From (10) and (11), it is clear that $\mathbf{E}_k$ is the only channel through which $\boldsymbol{\theta}$ is inferred from data.

The expression of $\mathbf{E}_k$ will be derived in Section 3.2, following conventional techniques of TMD dynamics. A parameter scheme is proposed so that the set of parameters can be uniquely identified, i.e., 'globally identifiable' in a Bayesian context [34]. In this case, the posterior PDF has a centralised distribution with a unique maximum in the admissible domain of $\boldsymbol{\theta}$. Using a second-order Taylor approximation of the NLLF, the posterior PDF can be approximated by a Gaussian PDF centred at the most probable value (MPV) and with a (posterior) covariance matrix. The MPV is analogous to the 'best' estimate in non-Bayesian methods. The posterior covariance matrix measures the identification uncertainty of parameters that remains despite the availability of data. Mathematically, the MPV maximises the likelihood function, or equivalently, minimises the NLLF. An Expectation-Maximisation (EM) algorithm is proposed in Section 4.1 for efficient determination of the MPV, which is otherwise computationally prohibitive because of the potentially large number of parameters and their implicit nonlinear influence on the NLLF. On the other hand, the posterior covariance matrix is mathematically equal to the inverse of Hessian of the NLLF at the MPV, whose efficient computation based on analytical expressions of derivatives will be discussed in Section 4.2.

3.2 Theoretical PSD matrix of response data with TMD

Consider a classically damped MDOF structure with mass matrix $\mathbf{M}_p$, stiffness matrix $\mathbf{K}_p$, damping matrix $\mathbf{C}_p$ and displacement vector $\mathbf{x}$, subjected to force vector $\mathbf{F}$; dependence of $\mathbf{x}$ and $\mathbf{F}$ on time t has been omitted for simplicity. The structure is installed with a TMD with mass m_d, stiffness k_d and damping c_d. The dynamics of the TMD is modelled by a single displacement DOF υ relative to a generalised coordinate $y = \mathbf{L}^T\mathbf{x}$ of the primary structure so that the kinetic, strain and dissipated energy of the TMD are given by $m_d(\dot{y}+\dot{\upsilon})^2/2$, $k_d\upsilon^2/2$ and $c_d\dot{\upsilon}^2/2$, respectively. Here, $\mathbf{L}$ is a vector involved in the generalised definition of TMD action, which need not be equal to a conventional location matrix. When the TMD is aligned with a particular DOF of the structure, $\mathbf{L}$ is simply a column vector with the only non-zero entry being 1 at that DOF. This particular case is depicted in Figure 3. In the general case (as will be seen shortly), with a proper parameter scheme, it is not necessary to know $\mathbf{L}$, which may not be available in precise form in field applications. In this sense, the dynamics and properties of the TMD have been modelled/defined in a general manner without specific reference to how the TMD is connected to the structure so that the proposed methodology can be applied in a robust way without such information.

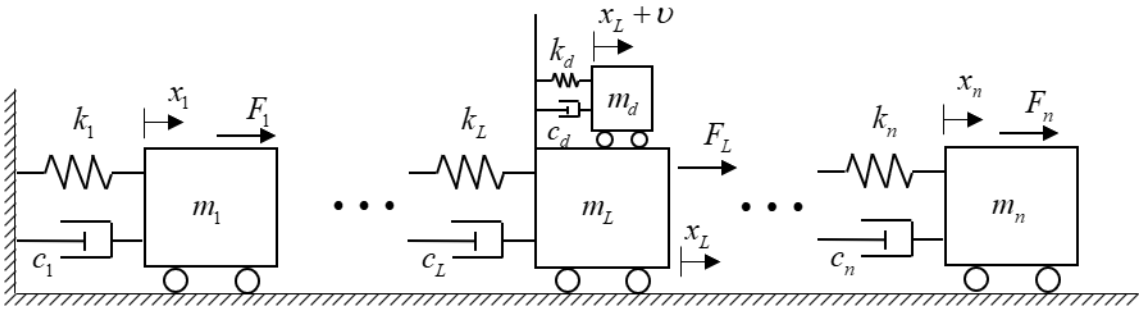

Figure 3 Schematic diagram of a structure-TMD system, illustrated for the special case of masses connected in series and a TMD is aligned with the *L*-th DOF. In this case, $y = x_L$ and $\mathbf{L}$ is a column vector with the only non-zero entry equal to 1 at the *L*-th entry.

Analogous to (1) and (2), the equations of motion of the structure and the TMD are respectively given by

$$\mathbf{M}_p\ddot{\mathbf{x}} + \mathbf{C}_p\dot{\mathbf{x}} + \mathbf{K}_p\mathbf{x} + m_d\mathbf{L}(\mathbf{L}^T\ddot{\mathbf{x}} + \ddot{\upsilon}) = \mathbf{F} \tag{12}$$

$$m_d\ddot{\upsilon} + c_d\dot{\upsilon} + k_d\upsilon = -m_d\mathbf{L}^T\ddot{\mathbf{x}} \tag{13}$$

To understand these equations, first note that (13) is the familiar equation of SDOF (relative) motion subjected to base acceleration $\mathbf{L}^T\ddot{\mathbf{x}}$. For (12), the term $m_d\mathbf{L}(\mathbf{L}^T\ddot{\mathbf{x}}+\ddot{\upsilon})$ is the interactive force from TMD on the primary structure. It results directly when the equation is derived via Lagrangian dynamics, or otherwise can be understood from (13) as resulting from the damping and stiffness force of the TMD, i.e., $c_d\dot{\upsilon}+k_d\upsilon=-m_d(\mathbf{L}^T\ddot{\mathbf{x}}+\ddot{\upsilon})$. The vector $\mathbf{L}$ can be viewed as projecting the damping and stiffness force of the TMD to the primary structure DOFs. The detail of $\mathbf{L}$ is not important as it does not need to be identified directly (see later). It can be shown that (12) and (13) reduce to (1) and (2) when the primary structure has only one DOF because then $\mathbf{L}=1$.

Following a similar approach in arriving at (5), the FT of $\ddot{\upsilon}$ can be expressed in terms of the FT of $\ddot{x}$ as $\mathcal{F}_{\ddot{\upsilon}}=-h_d\mathbf{L}^T\mathcal{F}_{\ddot{\mathbf{x}}}$, where h_d (except for a sign) is the FRF between the generalised acceleration $\ddot{y}=\mathbf{L}^T\ddot{\mathbf{x}}$ and $\ddot{\upsilon}$, i.e., (6) as in the SDOF case. Substituting this expression into the FT of (12) and using $\mathcal{F}_{\dot{\mathbf{x}}}=(\mathbf{i}\omega)^{-1}\mathcal{F}_{\ddot{\mathbf{x}}}$ and $\mathcal{F}_{\mathbf{x}}=-\omega^{-2}\mathcal{F}_{\ddot{\mathbf{x}}}$ gives

$$[\mathbf{M}_p+(\mathbf{i}\omega)^{-1}\mathbf{C}_p-\omega^{-2}\mathbf{K}_p+m_d(1-h_d)\mathbf{L}\mathbf{L}^T]\mathcal{F}_{\ddot{\mathbf{x}}}=\mathcal{F}_{\mathbf{F}} \tag{14}$$

where $\mathcal{F}_{\mathbf{F}}$ denotes the FT of $\mathbf{F}$ and ω is the FT frequency variable. Rearranging terms gives an expression of $\mathcal{F}_{\ddot{\mathbf{x}}}$ involving $\mathbf{M}_p$, $\mathbf{C}_p$ and $\mathbf{K}_p$. We will next make use of mode shape orthogonality of the classical damped primary structure to obtain expressions directly in terms of modal properties.

Consider a selected resonance band dominated by the subject modes of interest. The FT of acceleration response in the band can then be approximated (by ignoring other modes) as $\mathcal{F}_{\ddot{\mathbf{x}}}=\boldsymbol{\psi}\mathcal{F}_{\ddot{\boldsymbol{\eta}}}$, where $\boldsymbol{\psi}=[\boldsymbol{\psi}_1,...,\boldsymbol{\psi}_m]$ contains the subject mode shapes in its columns, i.e., $\mathbf{K}_p\boldsymbol{\psi}_i=(2\pi f_i)^2\mathbf{M}_p\boldsymbol{\psi}_i\ \ (i=1,...,m)$ with f_i (Hz) being the corresponding natural frequency and m being the number of modes dominating the resonance band; $\ddot{\boldsymbol{\eta}}=[\ddot{\eta}_1,...,\ddot{\eta}_m]^T$ is a vector of modal acceleration responses. Assuming that the primary structure is classically damped, the mode shapes are orthogonal with respect to the stiffness, damping and mass matrix, i.e., $\boldsymbol{\psi}_i^T\mathbf{K}_p\boldsymbol{\psi}_j=\boldsymbol{\psi}_i^T\mathbf{C}_p\boldsymbol{\psi}_j=\boldsymbol{\psi}_i^T\mathbf{M}_p\boldsymbol{\psi}_j=0$ whenever $i\neq j$ and each $\eta_i\ (i=1,...,m)$ satisfies its own SDOF equation of motion uncoupled from other modes.

Substituting $\mathcal{F}_{\ddot{\mathbf{x}}} = \boldsymbol{\psi}\mathcal{F}_{\ddot{\boldsymbol{\eta}}}$ into (14), pre-multiplying by $[\boldsymbol{\psi}^T\mathbf{M}_p\boldsymbol{\psi}]^{-1}\boldsymbol{\psi}^T$ and rearranging gives the FT of modal acceleration response as

$$\mathcal{F}_{\ddot{\boldsymbol{\eta}}} = [\mathbf{h}^{-1} + (1-h_d)\mathbf{r}\mathbf{b}\mathbf{b}^T]^{-1}\mathcal{F}_{\mathbf{w}} \tag{15}$$

where $\mathcal{F}_{\mathbf{w}}$ denotes the FT of the modal force vector (per unit modal mass) $\mathbf{w}$

$$\mathbf{w} = [\boldsymbol{\psi}^T\mathbf{M}_p\boldsymbol{\psi}]^{-1}\boldsymbol{\psi}^T\mathbf{F} \tag{16}$$

$$\mathbf{b} = \boldsymbol{\psi}^T\mathbf{L} \tag{17}$$

and $\mathbf{h}$ is a diagonal matrix of modal FRFs h_i, where $h_i = [1-\beta_i^2 - 2\zeta_i\beta_i\mathbf{i}]^{-1}$ and $\beta_i = f_i / \mathrm{f}_k$ is a frequency ratio; f_i (Hz) and ζ_i are respectively the natural frequency and damping ratio of mode i; $\mathbf{r}$ is a diagonal matrix of (modal) TMD mass ratio r_i where $r_i = m_d \big/ \boldsymbol{\psi}_i^T\mathbf{M}_p\boldsymbol{\psi}_i$.

The final step in the derivation is to relate the FT of modal response to that of the measured data. Let $\boldsymbol{\varphi}_i$ be the *i*-th mode shape confined to the measured DOFs only. The FT of measured acceleration data in the selected band is then modelled as $\mathcal{F}_{\hat{\ddot{\mathbf{x}}}} = \boldsymbol{\Phi}\mathcal{F}_{\ddot{\boldsymbol{\eta}}} + \boldsymbol{\varepsilon}$ where $\boldsymbol{\Phi} = [\boldsymbol{\varphi}_1, ..., \boldsymbol{\varphi}_m]$ comprises the mode shapes (confined to measured DOFs) in its columns and $\boldsymbol{\varepsilon}$ is the FT of measurement noise, assumed to be independent and identically distributed (i.i.d.) among different channels with a common PSD S_e and independent from the modal force (per unit modal mass) $\mathbf{w}$. The PSD matrix of acceleration data measured from structure (with TMD) is then given by

$$\mathbf{E} = E[\mathcal{F}_{\hat{\ddot{\mathbf{x}}}}\mathcal{F}_{\hat{\ddot{\mathbf{x}}}}^*] = \boldsymbol{\Phi}[\mathbf{h}^{-1} + (1-h_d)\mathbf{r}\mathbf{b}\mathbf{b}^T]^{-1}\mathbf{S}\,[\mathbf{h}^{-1} + (1-h_d)\mathbf{r}\mathbf{b}\mathbf{b}^T]^{-*}\boldsymbol{\Phi}^T + S_e\mathbf{I}_n \tag{18}$$

where $\mathbf{S} = E[\mathcal{F}_{\mathbf{w}}\mathcal{F}_{\mathbf{w}}^*]$ is the modal force PSD; the superscript '-*' denotes the conjugate transpose of the inverse of the subject matrix. The dependence of $\mathbf{E}$, $\mathbf{h}$ and h_d on the FT frequency f_k has been omitted for simplicity in notation. Note that the PSD matrix now accounts for non-classically damped modal dynamics resulting from the combined structure-TMD system, where $\mathbf{h}^{-1} + (1-h_d)\mathbf{r}\mathbf{b}\mathbf{b}^T$ in the PSD matrix $\mathbf{E}$ may not be a diagonal matrix and the frequency response characteristics in a narrow band will be the same as Figure 2 in Section 2.1. The term $\mathbf{E}$ reduces to the PSD matrix in the nominal case (i.e., without TMD) only when all the elements in $(1-h_d)\mathbf{r}\mathbf{b}\mathbf{b}^T$ are zero.

3.3 Identifiability and proposed parameter scheme

The parameters to be identified in the OMA problem of the structure-TMD system are those that affect the data PSD matrix $\mathbf{E}$ in (18). As in the nominal case (i.e., without TMD), they include the natural frequencies $\{f_i\}_{i=1}^m$, damping ratios $\{\zeta_i\}_{i=1}^m$, modal force PSD matrix $\mathbf{S}$, and noise PSD S_e. With the introduction of TMD, there are additional parameters arising from the properties of TMD $\{f_d, \zeta_d\}$, the $(m \times m)$ diagonal matrix $\mathbf{r}$ (related to TMD/modal masses) and $\mathbf{b}$ (related to the orientation/installation of TMD).

Ideally, modal parameters should be identified based on (18) since it strictly follows the model. However, an initial investigation on (18) revealed that the presence of $\mathbf{r}$ and $\mathbf{b}$ can potentially render the problem unidentifiable. In order to make the problem globally identifiable, attempts have been made to come up with a reduced set of parameters. An important finding is that when $\mathbf{b}\mathbf{b}^T$ is a diagonal matrix, $\mathbf{r}$ and $\mathbf{b}\mathbf{b}^T$ can be combined into a diagonal matrix, for which it can be reasoned (and verified numerically) that the problem is globally identifiable. Under this condition, it can be seen from (15) that the FT of the *i*-th modal response is only related to the FT of the *i*-th modal force. For this reason, we refer the condition as 'independent tuning'. By noting from (17) that $\mathbf{b}\mathbf{b}^{\mathrm{T}} = \boldsymbol{\psi}^{\mathrm{T}}\mathbf{L}\mathbf{L}^{\mathrm{T}}\boldsymbol{\psi}$, the condition requires that $\mathbf{L}\mathbf{L}^T$ is diagonalisable by the mode shapes. The mathematical condition for this assumption is the same as that for the classical damping matrix $\mathbf{C}_p$ [43,44], i.e., $\mathbf{K}_p\mathbf{M}_p^{-1}\mathbf{L}\mathbf{L}^T = \mathbf{L}\mathbf{L}^T\mathbf{M}_p^{-1}\mathbf{K}_p$. Nevertheless, such mathematical condition is of little substance or out of context because it is difficult (if possible) to check; the physical basis for this condition is also questionable. This condition will be applied as an empirical approximation so that the problem is globally identifiable. The issue of relevance then lies in whether this approximation will significantly bias the identification results, which will be investigated numerically in Section 5.

Assuming that $\mathbf{b}\mathbf{b}^T$ is a diagonal matrix (independent tuning), it can be combined with $\mathbf{r}$ (also a diagonal matrix) to form the diagonal matrix $\mathbf{r}\mathbf{b}\mathbf{b}^T$ with diagonal elements $\{\mu_i\}_{i=1}^m$ where

$$\mu_i = \frac{(\boldsymbol{\psi}_i^T\mathbf{L})^2}{\boldsymbol{\psi}_i^T\mathbf{M}_p\boldsymbol{\psi}_i} m_d \tag{19}$$

This is referred to as the (generalised) 'modal TMD mass ratio', which depends on the ratio of TMD to modal mass as well as how the TMD is oriented/installed. It is seen that $\mathbf{L}$ is just one of the unknown terms in (19), so even knowing the information about $\mathbf{L}$ may not increase the

identification precision since other terms (e.g., m_d) are still unknown. Clearly, if a mode i is not affected by the TMD then $\mu_i = 0$. Substituting (19) into (15) and noting that $\mathcal{F}_{\ddot{\mathbf{x}}} = \boldsymbol{\psi}\mathcal{F}_{\ddot{\boldsymbol{\eta}}}$, one obtains $\mathcal{F}_{\ddot{\mathbf{x}}} = \Sigma_{i=1}^{m}\boldsymbol{\psi}_i g_i \mathcal{F}_{w_i}$, where $\mathcal{F}_{w_i}$ is the FT of the *i*-th modal force; g_i is modal FRF reflecting the aggregate effect of TMD and primary structure:

$$g_i = [1-\beta_i^2 + \mu_i(1-h_d) - 2\zeta_i\beta_i\mathbf{i}]^{-1} \qquad \beta_i = f_i / \mathrm{f}_k \tag{20}$$

Correspondingly, the PSD matrix of data in (18) at f_k can be written in its final form as

$$\mathbf{E}_k = E[\mathcal{F}_{\hat{\ddot{\mathbf{x}}}}\mathcal{F}_{\hat{\ddot{\mathbf{x}}}}^*] = \boldsymbol{\Phi}\mathbf{H}_k\boldsymbol{\Phi}^T + S_e\mathbf{I}_n \tag{21}$$

where $\mathbf{H}_k = \mathbf{g}_k\mathbf{S}\mathbf{g}_k^*$; $\mathbf{g}_k$ is a diagonal matrix containing the FRFs g_i. In summary, the set of modal parameters to be identified includes

$$\{f_i\}_{i=1}^m, \{\zeta_i\}_{i=1}^m, \{\mu_i\}_{i=1}^m, f_d, \zeta_d, \boldsymbol{\Phi}, \mathbf{S}, S_e \tag{22}$$

where f_d (Hz) and ζ_d are respectively the natural frequency and damping ratio of TMD.

Although the theoretical PSD matrix of measured data in (21) has the same mathematical form as the one in the ordinary case (i.e., without TMD), the modal FRFs g_i now account for the effect of TMD. In the next section, an Expectation-Maximisation (EM) algorithm will be presented for efficiently computing the MPV of parameters in (22).

4 Algorithms

In this section, Expectation-Maximisation (EM) algorithm is employed to develop an efficient algorithm for computing the MPV of modal parameters (Section 4.1), which has been used before to develop algorithms for ordinary case (i.e., without TMD) [45,46]. The application of EM in other OMA methods can be found in, e.g., [47–49]. In Section 4.2, analytical expressions for Hessian matrix are derived, allowing the posterior uncertainty to be determined in an accurate and efficient manner.

4.1 EM algorithm for determining most probable value

This section presents an EM algorithm for efficient computation of the MPV of parameters that minimises the NLLF function in (11). It is applicable for the general case of multiple (possibly close) modes in the selected band. The algorithm presented here can be viewed as an extension of [45] to account for TMD dynamics (through the new FRF), with additional parameters

$\{f_d, \zeta_d, \mu_1 \ldots \mu_m\}$ in the parameter set $\boldsymbol{\theta}$. For completeness, the EM algorithm extended to incorporate TMD parameters is briefly outlined here, focusing on the key questions required in the theory/implementation. Further details can be referred to [45].

EM algorithm [50] comprises two steps, i.e., the E-step (expectation) and M-step (maximisation). The E-step involves evaluating the expectation of the complete-data log-likelihood, i.e., $Q(\boldsymbol{\theta}\left|\boldsymbol{\theta}^{(\mathrm{t})}\right.) = \mathrm{E}_{\mathbf{Z}\left|\mathbf{X},\theta^{(\mathrm{t})}\right.}[\mathrm{L}(\boldsymbol{\theta}\left|\{\mathbf{X},\mathbf{Z}\}\right.]$, where $\mathbf{Z}$ is a (suitably chosen; see shortly) 'latent variable'; t (= 0, 1, 2,…) denotes the iteration number; and $\mathrm{E}_{\mathbf{Z}\left|\mathbf{X},\theta^{(\mathrm{t})}\right.}[\cdot]$ denotes an expectation taking over $\mathbf{Z}$ following its distribution conditional on observed data $\mathbf{X}$ and the estimate $\boldsymbol{\theta}^{(\mathrm{t})}$ of $\boldsymbol{\theta}$ in the current iteration. In the M-step, Q is maximised with respect to $\boldsymbol{\theta}$ to yield an update estimate $\boldsymbol{\theta}^{(\mathrm{t}+1)}$ for the next iteration, i.e., symbolically, $\boldsymbol{\theta}^{(\mathrm{t}+1)} = \arg\max_{\theta} Q(\boldsymbol{\theta}\left|\boldsymbol{\theta}^{(\mathrm{t})}\right.)$. Efficient implementation of the EM algorithm hinges on a proper choice (if possible) of the latent variable $\mathbf{Z}$ in the problem so that the expectation Q in the E-step can be efficiently calculated (ideally, analytically) for arbitrary values of $\boldsymbol{\theta}$ so that it can be optimised efficiently to yield the next estimate $\boldsymbol{\theta}^{(\mathrm{t}+1)}$ in the M-step. In the proposed EM algorithm (same as [45]), the latent variable is chosen as the FT of modal acceleration vector $\ddot{\boldsymbol{\eta}}_k$. The complete-data log-likelihood is given by

$$\begin{aligned}\mathrm{L}(\boldsymbol{\theta}\left|\{\hat{\mathcal{F}}_k, \ddot{\boldsymbol{\eta}}_k\}\right.) &= \sum \log p(\hat{\mathcal{F}}_k, \ddot{\boldsymbol{\eta}}_k \left|\boldsymbol{\theta}\right.) \\ &= -2nN_f \log \pi - nN_f \log S_e - S_e^{-1} \sum \left[\hat{\mathcal{F}}_k - \boldsymbol{\Phi}\ddot{\boldsymbol{\eta}}_k\right]^* \left[\hat{\mathcal{F}}_k - \boldsymbol{\Phi}\ddot{\boldsymbol{\eta}}_k\right] + \sum \log \left|\mathbf{H}_k^{-1}\right| - \sum \ddot{\boldsymbol{\eta}}_k^* \mathbf{H}_k^{-1} \ddot{\boldsymbol{\eta}}_k\end{aligned} \tag{23}$$

Taking expectation over $\ddot{\boldsymbol{\eta}}_k$ conditional on the $\boldsymbol{\theta}^{(\mathrm{t})}$ and $\{\hat{\mathcal{F}}_k\}$, and using standard formulae of conditional mean and variance of Gaussian variates gives the function Q

$$Q(\boldsymbol{\theta}\left|\boldsymbol{\theta}^{(\mathrm{t})}\right.) = -2nN_f \log \pi - nN_f \log S_e - S_e^{-1} Q_1(\boldsymbol{\theta}\left|\boldsymbol{\theta}^{(\mathrm{t})}\right.) + Q_2(\boldsymbol{\theta}\left|\boldsymbol{\theta}^{(\mathrm{t})}\right.) \tag{24}$$

where

$$Q_1(\boldsymbol{\theta}\left|\boldsymbol{\theta}^{(\mathrm{t})}\right.) = \sum \left\{\hat{\mathcal{F}}_k^* \hat{\mathcal{F}}_k - 2tr\left[\boldsymbol{\Phi}\,\mathrm{Re}(\mathbf{w}_{1k}\hat{\mathcal{F}}_k^*)\right] + tr\left[\boldsymbol{\Phi}\,\mathrm{Re}(\mathbf{w}_{2k})\boldsymbol{\Phi}^T\right]\right\} \tag{25}$$

$$Q_2(\boldsymbol{\theta}\left|\boldsymbol{\theta}^{(t)}\right.) = \sum \log\left|\mathbf{H}_k^{-1}\right| - tr\left[\sum \mathbf{H}_k^{-1}\mathbf{w}_{2k}\right] \tag{26}$$

where $\mathbf{w}_{1k} = E_{\ddot{\boldsymbol{\eta}}_k|\hat{\mathcal{F}}_k,\boldsymbol{\theta}^{(t)}}\left[\ddot{\boldsymbol{\eta}}_k\right]$ and $\mathbf{w}_{2k} = E_{\ddot{\boldsymbol{\eta}}_k|\hat{\mathcal{F}}_k,\boldsymbol{\theta}^{(t)}}\left[\ddot{\boldsymbol{\eta}}_k\ddot{\boldsymbol{\eta}}_k^*\right]$ are respectively the first and second conditional moments of $\ddot{\boldsymbol{\eta}}_k$ given $\hat{\mathcal{F}}_k$ and $\boldsymbol{\theta}^{(t)}$, which are computed by

$$\mathbf{w}_{1k} = \mathbf{J}_k^{-1}\boldsymbol{\Phi}^T\hat{\mathcal{F}}_k \qquad \mathbf{w}_{2k} = \mathbf{J}_k^{-1}\boldsymbol{\Phi}^T\hat{\mathcal{F}}_k\hat{\mathcal{F}}_k^*\boldsymbol{\Phi}\mathbf{J}_k^{-*} + S_e\mathbf{J}_k^{-1} \tag{27}$$

where $\mathbf{J}_k = S_e\mathbf{H}_k^{-1} + \boldsymbol{\Phi}^T\boldsymbol{\Phi}$. The terms $\mathbf{w}_{1k}$ and $\mathbf{w}_{2k}$ are constant in the M-step since they are evaluated at parameter values obtained in the previous iteration.

Following the similar procedure in [45], it can be shown that $\boldsymbol{\Phi}$, S_e and $\mathbf{S}$ can be respectively updated by (28)-(30):

$$\boldsymbol{\Phi} = \sum \mathrm{Re}(\hat{\mathcal{F}}_k\mathbf{w}_{1k}^*)\left[\sum \mathrm{Re}(\mathbf{w}_{2k})\right]^{-1} \tag{28}$$

$$S_e = \frac{Q_1(\boldsymbol{\theta}\left|\boldsymbol{\theta}^{(t)}\right.)}{nN_f} \tag{29}$$

$$\mathbf{S} = \frac{1}{N_f}\left(\sum \mathbf{g}_k^{-1}\mathbf{w}_{2k}\mathbf{g}_k^{-*}\right) \tag{30}$$

As a remark, in the M-step the mode shape matrix $\boldsymbol{\Phi}$, modal force PSD matrix $\mathbf{S}$ and noise PSD S_e can be optimised analytically in terms of the remaining parameters $\{f_i, \zeta_i, \mu_i, f_d, \zeta_d\}$. The remaining parameters are updated by optimising (26) numerically using black-box algorithms (e.g., simplex search [45]).

The iterative algorithm developed requires a proper initial guess of the parameters to start. Generally, the initial guess can be obtained as rough estimates of parameters from empirical quantities obtained in the initial phase of data analysis, such as the singular value (SV) spectrum of the measured data [51,52]. The excitation is assumed to be broadband near the resonance band of the modes so that the frequency characteristics of the SV spectrum give a direct reflection of dynamic amplification. An analytical investigation has been performed in Appendix A, which leads to the recommended initial guess method below:

1. Locate the peaks of the SV spectrum as the initial guess for the natural frequencies $\{\tilde{f}_i\}_{i=1}^2$ of the combined structure-TMD system; locate the trough as the TMD frequency f_d.

2. Calculate the initial guess for natural frequency of the mode tuned by TMD as $f_1 \approx \tilde{f}_1 \tilde{f}_2 / f_d$.
3. Calculate the initial guess for the TMD mass ratio as $\mu \approx \left[(\tilde{f}_1 - \tilde{f}_2)^2 - (f_1 - f_d)^2 \right] \Big/ f_d^2$.
4. Take the initial guess for ζ_1 as 1% (as in BAYOMA).
5. Calculate the initial guess for ζ_d based on the trough/peak ratio, as shown in (46) in Appendix A.2. If the calculated value of ζ_d is unreasonable (e.g., greater than 1), one may take $\zeta_d = 2\%$, which is slightly larger than the initial guess of ζ_1.
6. Set the initial guess for mode shape as the eigenvector (corresponding to the largest eigenvalue) of the real part of sample PSD matrix of data at the initial guess of natural frequency.
7. Calculate the initial guess of noise PSD using (29) based on high signal-to-noise asymptotics, together with the initial guess of modal properties calculated above. When the signal-to-noise ratio is high, $\mathbf{J}_k = S_e \mathbf{H}_k^{-1} + \boldsymbol{\Phi}^T \boldsymbol{\Phi} \sim \boldsymbol{\Phi}^T \boldsymbol{\Phi}$ ~, for which the second moment $\mathbf{w}_{2k}$ in (27) can be obtained directly. The initial guess of modal force PSD is then calculated using (30).

Some comments are in order regarding the above recommendation. The natural frequencies $\{\tilde{f}_i\}_{i=1}^2$ of the combined structure-TMD system and the natural frequency of the TMD f_d are estimated respectively from the peaks and trough of the SV spectrum during initial data analysis. Since $\{\tilde{f}_i\}_{i=1}^2$ and f_d are located from the SV spectrum as the peaks and trough locations, $\tilde{f}_1 \le f_d \le \tilde{f}_2$ and so the formula $f_1 \approx \tilde{f}_1 \tilde{f}_2 / f_d$ guarantees that the initial guess of f_1 will always lie between the two peaks. This formula suggests that the initial guess of f_1 should be close to the first peak ($\tilde{f}_1$) if the trough (f_d) is closer to the second peak ($\tilde{f}_2$); and vice versa. The above procedure is derived based on the case with a single mode tuned by a TMD. When there are close modes tuned by a TMD, one may simply repeat Steps 1-4 to set the initial guess of f_i, ζ_i and μ_i for other modes.

It should be noted that the above strategy for setting initial guess is not applicable for the case with large TMD damping ratio (e.g., a single peak with $\zeta_d = 16\%$ in Figure 2) because characteristic features in the SV spectrum, such as the trough, are absent. In such cases, one

may set the initial guess as the design value if such information is available. Otherwise, they can be roughly set from the SV spectrum as follows.

1. Set the peak of the SV spectrum as the initial guess for the primary structure f_1, and the TMD frequency f_d as $0.98 f_1$.
2. Set the initial guess for both ζ_1 and μ as 0.1%, and the initial guess for ζ_d as 1%.
3. Calculate the initial guess for other parameters (e.g., S_e) in the same way as Steps 6-7 in the case with small value of TMD damping ratio.

4.2 Identification uncertainty

This section investigates the identification uncertainty of the modal parameters in terms of their posterior covariance matrix. In a Bayesian context, the posterior covariance matrix is mathematically approximated by the inverse of the Hessian of the NLLF evaluated at the MPV of modal parameters. As mentioned in Section 3, the NLLF for the structure-TMD system in (11) has a similar form as that for the structure without TMD (see Equation (13.2) in [33]), except that the FRF **g** now accounts for the effect of TMD and contains additional TMD-related parameters $\{f_d, \zeta_d, \mu_1 \ldots \mu_m\}$. As a result, the framework for systematically determining the posterior covariance matrix in the ordinary case (i.e., without TMD) developed in Section 13.7 of [33] can still serve for the current case. See Figure 13.3 in [33] for the information flow of derivative calculations. The difference mainly lies in the derivatives of $\mathbf{H}_k$, which depend on the derivatives of the modal FRF *g*. Their derivatives are respectively summarised in Tables 4 and 5 of Appendix C.

5 Verification with synthetic data

In this section, examples based on synthetic data are presented to verify the proposed method and investigate the effect of modelling errors. Consider the horizontal vibration measured on a ten-storey shear building, which is equipped with a TMD installed on the top floor. The shear building (primary structure) has a uniform mass of 100 tonnes per floor, interstory stiffness of $k_x = 177$ kN/mm along x-direction and $k_y = 195$ kN/mm along y-direction, and damping ratio of 1% in all modes. The structural response is simulated based on Newmark scheme. The first two modes of the shear building have natural frequencies of 1 Hz and 1.05 Hz, corresponding to the fundamental translational modes along x- and y-directions, respectively. The primary

structure is subjected to independent and identically distributed (i.i.d.) Gaussian excitations at all floor levels, with one-sided root PSD of $11.77\,\mathrm{N}/\sqrt{\mathrm{Hz}}$ and $7.85\,\mathrm{N}/\sqrt{\mathrm{Hz}}$ along x- and y-directions, respectively. The ambient acceleration data is measured at all $10\times 2 = 20$ DOFs and sampled at 100 Hz. It is contaminated by i.i.d. Gaussian white noise with a root PSD of 1 $\mu g/\sqrt{\mathrm{Hz}}$. The TMD has a physical mass ratio of 2% (i.e., $m_d = 20$ tonnes), which is designed to tune the first mode of the primary structure. The modal mass ratio μ, the optimal frequency ratio α_{opt} and the optimal damping ratio $\zeta_{d_{opt}}$ are respectively calculated to be 3.79%, 0.964 and 11.27% from (31) [14].

$$\mu = \frac{(\boldsymbol{\psi}_1^T \mathbf{L})^2}{\boldsymbol{\psi}_1^T \mathbf{M} \boldsymbol{\psi}_1} m_d \quad \alpha_{opt} = \frac{1}{1+\mu} \quad \zeta_{d_{opt}} = \sqrt{\frac{3\mu}{8(1+\mu)^3}} \tag{31}$$

According to the investigation in Section 2.1, depending on the modal properties of both primary structure and the TMD, there are different tuning types often visually indicated from the SV spectrum. To verify the accuracy of the proposed method to different tuning types, several cases are considered with different natural frequencies f_d and damping ratios ζ_d of the TMD. Specifically, we define two parameters λ_f and λ_ζ as the 'tuning index' to vary the TMD natural frequency f_d and damping ratio ζ_d so that they are given by

$$f_d = \lambda_f \alpha_{opt} f_1 \qquad \zeta_d = \lambda_\zeta \zeta_{d_{opt}} \tag{32}$$

The parameter λ_f is respectively set to be 0.95, 1 and 1.05 to reflect the various frequencies of the TMD. In each value of λ_f, λ_ζ is taken as 0.5, 1 and 1.5 to cover the three typical tuning scenarios. First, consider the TMD is installed along the x-direction with λ_f equal to 1. In this case, the term $\mathbf{bb}^T$ mentioned in Section 3.2 is a diagonal matrix and there is no modelling error with respect to the installation of TMD. Three values of λ_ζ equal to 0.5, 1 and 1.5 are respectively used to generated ambient data. Figure 4 shows their SV spectra, which are plotted by taking the eigenvalues of the averaged sample PSD matrices at different frequencies. Note that the averaging concept is used here merely for producing smooth spectra for better visualisation. It is not involved in the Bayesian methodology. When $\lambda_\zeta = 0.5$ (i.e., $\zeta_d < \zeta_{d_{opt}}$), an additional peak due to the action of TMD can be clearly observed in the SV spectrum. When $\lambda_\zeta = 1.5$ (i.e., $\zeta_d > \zeta_{d_{opt}}$), the SV spectrum has a similar shape as the ordinary one (i.e., without

TMD). The spectrum indicates that the noise level of the data is around $1\,\mu g/\sqrt{Hz}$, which checks with the value assumed. As the resonance bands of the first two modes overlap, they are identified in the same frequency band picked as $[0.7,\ 1.3]$ Hz. The band is selected so that the resonant hump visually drops to the background noise level beyond the range. The initial guess of the modal parameters is determined based on the procedure in Section 4.1. Note that the proposed method operates in the frequency domain where the contributions of different modes are naturally separated. The effect of TMD on higher modes that are not designed to be tuned is marginal and so they can be identified by conventional methods based on classical damping assumption. Their identification results are omitted here.

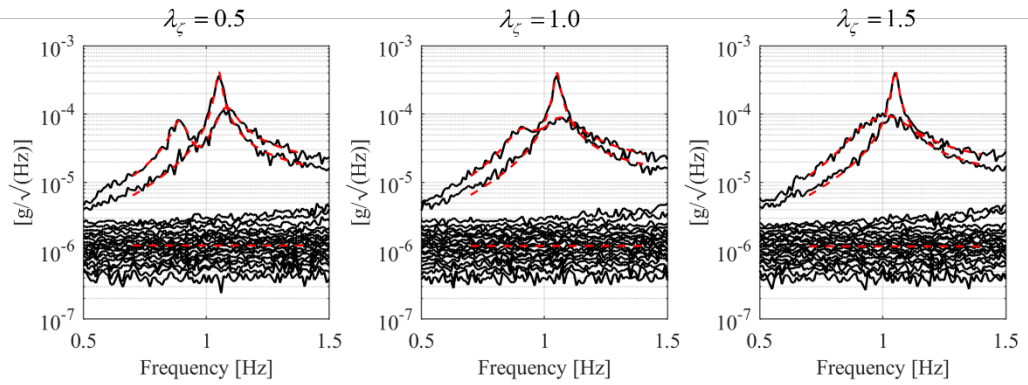

Figure 4 SV spectra of the three tuning types; dashed red line: theoretical SV at MPVs.

Table 1 summarises the identification results based on 20-min data durations, where the posterior c.o.v.s are shown in parenthesis. As can be seen, the identified MPVs are close to the exact values. In each case, the identified damping ratios and mass ratio have higher uncertainties compared with the identified natural frequencies. The uncertainties of the modal parameters for Mode 1 (which is tuned by TMD) are higher than their counterparts of Mode 2 (without the effect from TMD). For the modal parameters related to TMD (i.e., f_1, ζ_1, μ_1, f_d and ζ_d), their c.o.v.s generally increase with λ_ζ (hence the damping ratio of TMD). Modal parameters μ_1, ζ_1 and ζ_d have typically high c.o.v.s (> 50%) when the effect of TMD cannot be detected in the SV spectrum (i.e., $\lambda_\zeta = 1.5$). For large ζ_d, the SV spectrum is similar to the ordinary one (i.e., without TMD) and so it may not carry enough information to distinguish the TMD characteristics from those of the primary structure. The last two rows of Table 1 give the modal assurance criterion (MAC) between the most probable and exact mode shapes. All the values of MAC are close to unity, indicating that the mode shapes are identified with high

quality. The modal shape c.o.v.s of the two modes are of the same order of magnitude. The theoretical SV spectra calculated using the identified modal properties are shown in Figure 4 as dashed red lines, which generally fit the SV spectra calculated based on ambient data. The identification results of $\lambda_f = 0.95$ and $\lambda_f = 1.05$ are qualitatively similar as those of $\lambda_f = 1$, and details omitted here. For all the cases, the convergence tolerance in the iteration was set to be 10^{-5} on a fractional basis for all parameters. The calculation was performed using MATLAB R2019a on an HP EliteDesk 800G2 Desktop (Intel Core i5, 3.2 GHz and 8 GB of RAM). The computational time for determining MPV in the three cases shown in Figure 4 are 20.1, 19.7 and 23.8 seconds, respectively.

Table 1 Modal identification results, synthetic data.

Parameter	$\lambda_\zeta = 0.5$		$\lambda_\zeta = 1.0$		$\lambda_\zeta = 1.5$	
	MPV	Exact	MPV	Exact	MPV	Exact
f_1 [Hz]	1.001 (0.24%)	1.000	1.004 (0.34%)	1.000	0.998 (0.89%)	1.000
f_2 [Hz]	1.050 (0.09%)	1.050	1.051 (0.09%)	1.050	1.050 (0.09%)	1.050
f_d [Hz]	0.964 (0.25%)	0.964	0.964 (0.63%)	0.964	0.957 (2.33%)	0.964
ζ_1 [%]	0.97 (65%)	1.00	2.10 (60%)	1.00	2.12 (149%)	1.00
ζ_2 [%]	0.96 (10%)	1.00	1.01 (10%)	1.00	0.90 (10%)	1.00
ζ_d [%]	5.59 (10%)	5.64	9.84 (19%)	11.27	15.01 (52%)	16.91
μ_1 [%]	3.75 (8%)	3.79	3.18 (27%)	3.79	2.84 (105%)	3.79
$S_{11}\left[\mu g/\sqrt{Hz}\right]$	11.96 (5%)	12.00	12.33 (8%)	12.00	12.25 (14%)	12.00
$S_{22}\left[\mu g/\sqrt{Hz}\right]$	7.90 (3%)	8.00	8.09 (3%)	8.00	7.95 (3%)	8.00
$S_e\ \left[\mu g/\sqrt{Hz}\right]$	1.19 (0.7%)	1.00	1.18 (0.7%)	1.00	1.16 (0.7%)	1.00
Mode 1 MAC	1.000 (1.62%)	1.000	1.000 (1.97%)	1.000	1.000 (2.07%)	1.000
Mode 2 MAC	1.000 (2.17%)	1.000	1.000 (2.19%)	1.000	1.000 (2.18%)	1.000

We next investigate the uncertainty calculated by the proposed method from a statistical sense. For this purpose, 1000 i.i.d. data sets (20-min each) are generated in each case and 1000 results can be obtained in terms of MPV and posterior c.o.v.s accordingly. Table 2 compares the Bayesian and frequentist statistics of the identified frequencies, mass ratio and damping ratio of TMD. The column 'Freq.' (short for frequentist) shows the sample c.o.v.s of the MPVs among the 1000 i.i.d. data sets, which is calculated as the ratio of the sample standard deviation to the sample mean of the MPV. The column 'Bay.' (short for Bayesian) shows the sample root mean square (RMS) value of the posterior standard deviation divided by the sample mean of the MPV. It is seen that the Bayesian posterior c.o.v.s are in the same order of magnitude as their sample counterparts, but they are not exactly equal; they need not be. Based on the theory in [53], if there is no modelling error, up to a second-order approximation of the log-likelihood function, the ensemble average of posterior variance is approximately equal to the ensemble variance of MPV in a weighted sense. It should be noted that the identified damping ratio ζ_1 of the primary structure (not shown here) is occasionally quite small (say, in the order of 1e-13) in some data sets, especially in the cases with large ζ_d (i.e., $\lambda_\zeta = 1.5$). This could be due to the low sensitivity of ζ_1 to the NLLF when the damping ratio of TMD is large. However, the inaccuracy of ζ_1 does not affect the precision of other parameters (as shown in Table 2 and Figure 5 later) and it is hence less important because one is more concerned with the modal properties of TMD in practice.

Table 2 Sample and Bayesian statistics, synthetic data.

Parameter	$\lambda_\zeta = 0.5$		$\lambda_\zeta = 1.0$		$\lambda_\zeta = 1.5$	
	Freq. % (C)	Bay. % (D)	Freq. % (C)	Bay. % (D)	Freq. % (C)	Bay. % (D)
f_1 [Hz]	0.47	0.42	0.55	0.55	0.58	0.50
f_2 [Hz]	0.15	0.16	0.18	0.17	0.22	0.19
f_d [Hz]	0.46	0.44	1.88	1.72	5.19	4.84
ζ_d [%]	19	17	51	43	91	76
μ_1 [%]	15	13	63	53	100	81

The posterior uncertainty can also be assessed quantitatively from the recently developed 'uncertainty laws' [33]. For the present case, the natural frequency is around 1 Hz, and so the data contains 20 × 60 = 1200 natural periods. Using the uncertainty law formulae for close modes [54] (ignoring the presence of TMD) with the assumed bandwidth factor $\kappa = \text{bandwidth}\left(\text{Hz}\right)/2f_1\zeta_1 = 6$ and 'exact' value of modal parameters, one can obtain that the posterior c.o.v. of natural frequency is around 0.1% and the posterior c.o.v. of damping ratio is around 13%. This is consistent with the results of the second mode of the primary structure in Tables 1 and 2. For the modal parameters of the first mode and TMD, in addition to the common effects (e.g., data length, modal s/n ratio), their uncertainties also depend on whether the data contains enough information to distinguish TMD characteristics from those of primary structure. This is the reason why their uncertainties increase with the TMD damping ratio.

To further illustrate the consistency of the proposed method, Figure 5 shows the identified results of some parameters versus data length corresponding to the three typical scenarios. The dashed red lines denote the exact value. The identified results for each data duration are reported with a dot at the MPV and an error bar covering ± 2 posterior standard deviations. As the data duration increases, the error bar generally narrows. There is no evidence of bias since the error bar generally covers the exact values regardless of the data durations.

The proposed algorithm in this work assumes that the orientation/installation of the TMD satisfies the condition that $\mathbf{b}\mathbf{b}^T$ is a diagonal matrix. However, this need not be true in practice. For example, when the orientation of the TMD has an angle offset with the x-direction, modelling error exists in the model since $\mathbf{b}\mathbf{b}^T$ is no longer a diagonal matrix. Potential bias in the MPVs and posterior c.o.v.s is next investigated through a parametric study with synthetic data. Three values of λ_ζ are considered when TMD has optimal frequency (i.e., $\lambda_f = 1$). For each value of λ_ζ, four scenarios with increasing installation angles with respect to the x-direction are considered, i.e., 0°, 15°, 30° and 45°. Similar to the above investigation, 1000 i.i.d data sets (20-min each) are generated in each case and 1000 results are obtained in terms of the MPV and the posterior c.o.v.. The sample c.o.v. results are also obtained based on the 1000 results. In each data set, the frequency band is selected as $[0.7,1.3]$ Hz (same as before), and the initial guess of properties is determined based on the same procedure mentioned in Section 4.1.

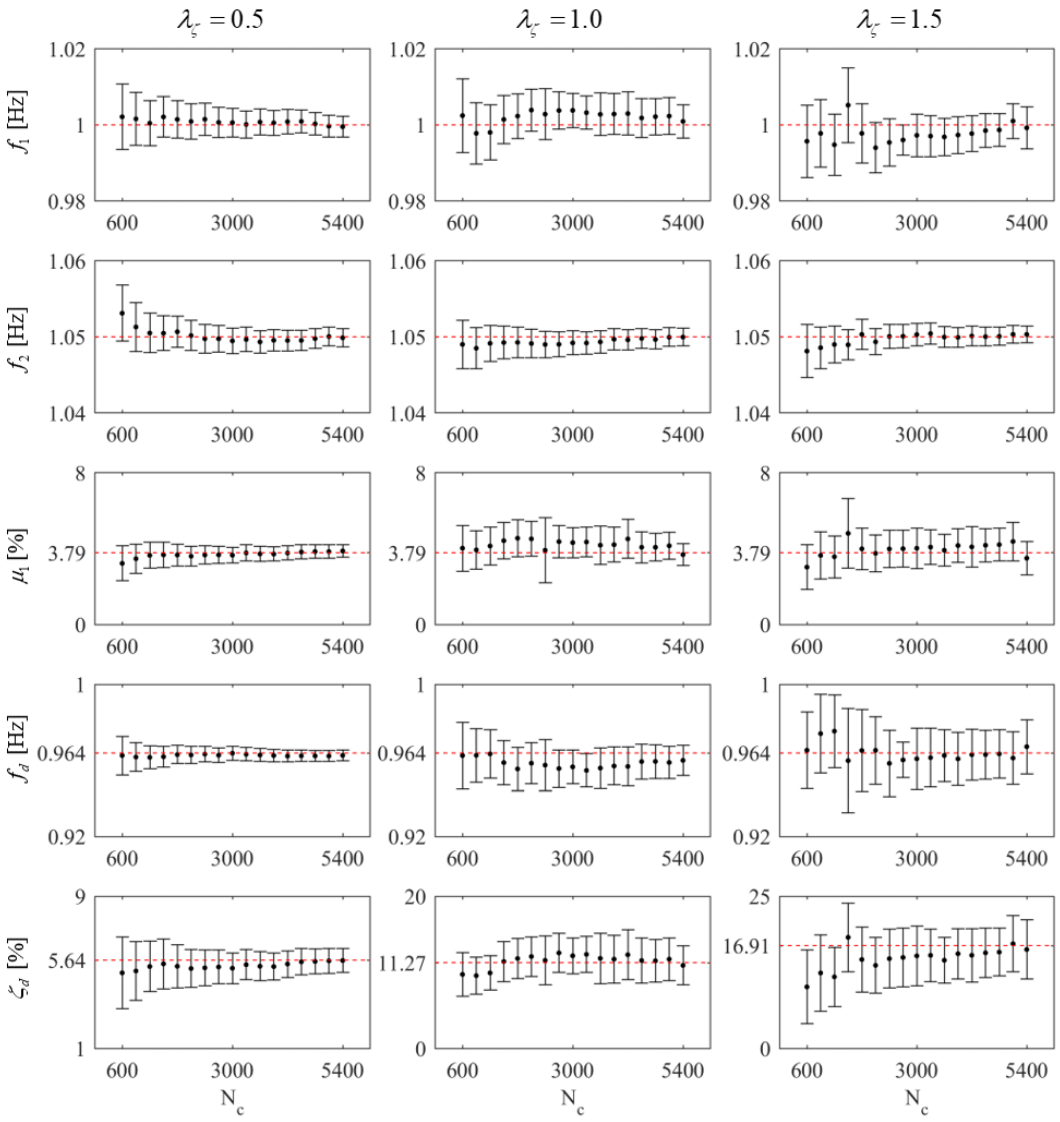

Figure 5 Identified modal properties vs N_c, synthetic data with $\lambda_f = 1$. N_c = data duration/natural period; dot: MPV; error bar: ±2 standard deviations; red dashed line: exact value.

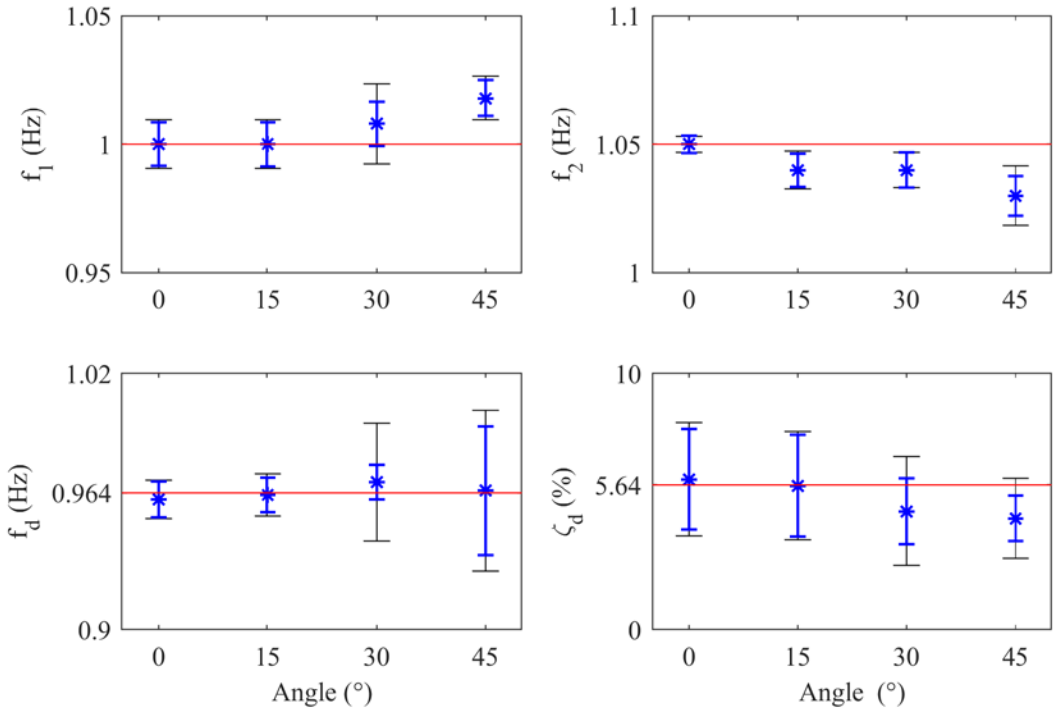

Figure 6 Identified modal properties vs TMD installation angle, synthetic data with $\lambda_f = 1$ and $\lambda_\zeta = 0.5$. Asterisk: sample mean value of the MPVs among 1000 i.i.d. data sets; blue error bar: ± 2 posterior standard deviations; black error bar: ± 2 sample standard deviations; red dashed line: exact value.

Figure 6 shows the results of identified natural frequencies and damping ratio of TMD for different installation angles. The identified results for each installation angle are reported with an asterisk at the sample mean of MPVs, a blue error bar covering ± 2 posterior standard deviations and a black error bar covering ± 2 sample standard deviations. The identified results of mass ratios are not presented since the exact values of mass ratios are absent in this case. Figure 6 shows that the sample c.o.v.s are generally higher than the posterior c.o.v.s, indicating the existence of modelling error in the identified results. There is no clear evidence that the identified TMD natural frequency f_d and damping ratio ζ_d have bias because the error bars generally cover the exact values. Bias can be observed in the results of the natural frequencies of the primary structure f_1 and f_2, although it is considered practically insignificant. Even in the extreme case of 45º in the angle offset, the bias is less than 2%. This indicates that the diagonal approximation of $\mathbf{b}\mathbf{b}^T$ does not significantly bias the identification results.

6 Application with field data

The proposed algorithm is next applied to the ambient vibration data of a chimney installed with a TMD system. The instrumented structure is a 183 m reinforced concrete chimney at the Rugeley Power Station, England, UK. The Rugeley chimney was constructed in 1968, which consisted of a tapered windshield with an external diameter of 15.7 m at the base and narrowing to 9.4 m at the top. In 2006, a replacement flue gas desulphurisation chimney was built with the same height in the vicinity of the old Rugeley chimney. The two chimneys (see Figure 2 in [12]) had coexisted for approximately two years before the old one was demolished. An investigation of cross-wind interference effects anticipated increased levels of wind-induced response to the old chimney. Following the recommendations of the study, a vibration monitoring system was installed [55,56]. A TMD was installed at 16 m from the top to improve the structural resistance of the old Rugeley chimney to the interference effects. Configuration is shown in Figure 7 in [12]. The TMD comprises 42,000 kg of a pendular moving mass (i.e., a hollow steel ring filled with concrete) hung by cables to tune the lowest harmonic vibration around 0.33 Hz. The moving mass is connected to the stack via five viscous damper units and allows a maximum relative displacement of 450 mm. Other parameters for the TMD are listed as follows: damping coefficient of 18 kNs/m, equivalent stiffness of 180 kN/m, and modal mass at TMD location of 1.28×10^{6} kg.

The investigation on TMD performance found that the TMD was not apparently engaged substantially during weak wind periods [12]. Hence, the analysis here will be based on a potential high wind period during 29-30 Mar 2008 (near two days period). The 46 hour data was divided into non-overlapping 20-min windows, within which modal properties are assumed to be time-invariant, and the data is assumed to be statistically stationary. Figure 7 shows the root PSD and the root SV spectrum of a typical 20-min data set. There is one resonance band shown around 0.3 Hz. Due to the symmetrical nature of the structure, the two modes are at quite close frequencies. A hump appears on the left side of the resonant peak due to the action of the TMD. The (hand-picked) frequency band is indicated by a horizontal bar '[-]'. The initial guess of natural frequencies, mass ratio and damping ratio are determined by the procedure in Section 4.1. Table 3 summarises the identification results based on a typical 20-min data segment. It can be seen that the natural frequencies f_1 and f_2 of the primary structure are quite close. The identified damping ratios of the primary structure are quite small (in the order of 1e-11) with significantly high uncertainties, as also encountered in the synthetic

example. The last row of Table 3 gives the equivalent damping ratios of the first two modes, which are calculated by (54) in Appendix B. The equivalent damping ratio is used as a proxy to reflect the energy dissipation capability of the TMD; see Appendix B for details. Figure 8 shows the identified most probable mode shapes projected onto the horizontal (XY) plane for the first two modes plotted with arrows pointing from the origin. It can be seen that Modes 1 and 2 appear to be perpendicular. To visualise the identification uncertainty, the dominant uncertainty of each mode is plotted in Figure 8 with a red line stemming from the tip of the most probable mode shape. This is obtained from the eigenvector (with the maximum eigenvalue) of the posterior covariance matrix of mode shape multiplied by the square root of the eigenvalue.

It should be noted that the identified results can differ from one data set to another due to the variability of modal parameters and identification uncertainty. Applying the same procedure to each 20-min data segment, we can track how the identified modal properties vary with time. Figure 9 shows the identified natural frequencies, damping ratios and mass ratios over different time windows. For the identified modal properties, the result in each time window is plotted with a dot at the MPV and an error bar covering ± 1 posterior standard deviation. Note that the damping ratios of Modes 1 and 2 are equivalent damping ratios, reflecting the damping level of the combined structure. The natural frequencies and modal mass ratios for the first two modes are close and exhibit similar trends. The equivalent damping ratios of Mode 1 stay above 2%, typically considered high. The natural frequency of TMD is lower than that of Mode 1 and Mode 2. Based on Figure 9 (a) and (b), it can be observed that some coincidence of low values in the natural frequencies, and high values in damping ratios, suggesting opposite trends. Figure 9 (b) and (c) show that the TMD damping ratio follows a similar trend as the modal mass ratio. Efforts have been made to investigate whether this is because of the amplitude-dependent properties of the parameters, but no systematic trend has been found between the amplitude and these parameters.

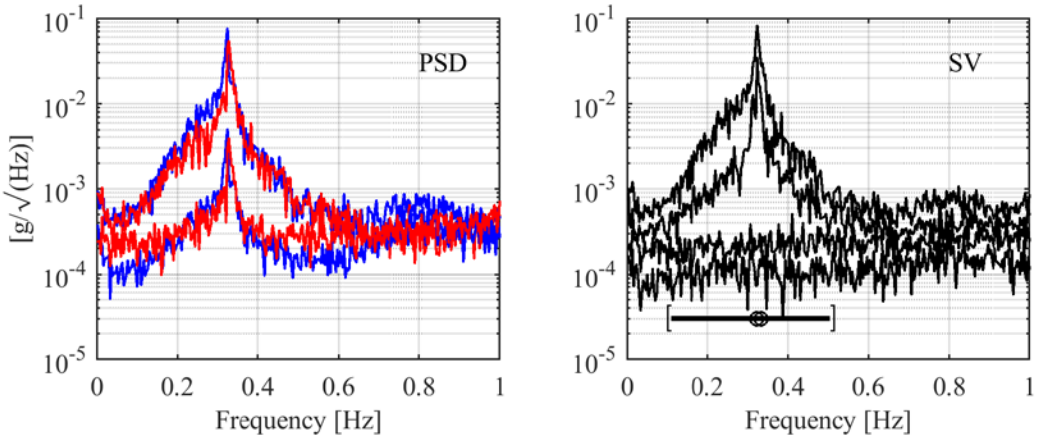

Figure 7 Root PSD and root SV spectra for a typical 20-min data; in PSD, blue line: x-direction, and red line: y-direction; in SV, horizontal bar '–' indicates the selected band for modal identification.

Table 3 Identified results MPV with c.o.v in parenthesis.

Parameter	Mode 1	Mode 2
Frequency f [Hz]	0.290 (0.53%)	0.310 (0.25%)
Damping ratio ζ [%]	2.03e-11(3.4e7%)	1.84e-11(1.4e7%)
Mass ratio μ [%]	6.14 (5%)	4.01 (8%)
TMD frequency f_d [Hz]	0.268 (0.94%)	
TMD damping ratio ζ_d [%]	5.94 (5%)	
Modal force PSD S_{ii} g^2 / Hz	8.301e-6 (5%)	1.132e-6 (4%)
Prediction error PSD S_e g^2 / Hz	5.002e-8 (3.3%)	
Equivalent damping ratio ζ_e [%]	4.56	2.28

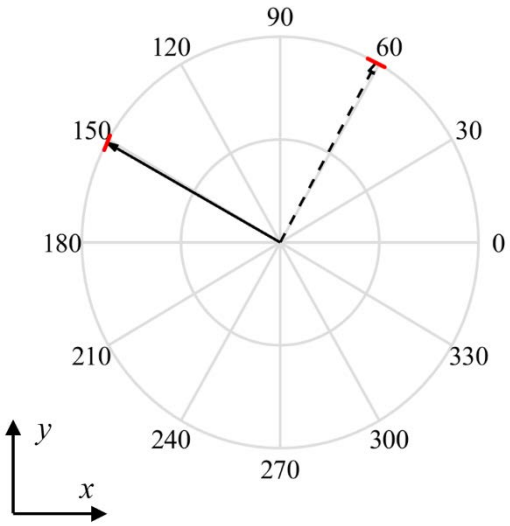

Figure 8 Identified most probable mode shapes (black lines) and their uncertainty along the dominant direction (red lines); the solid line for the first mode and the dashed line for the second mode.

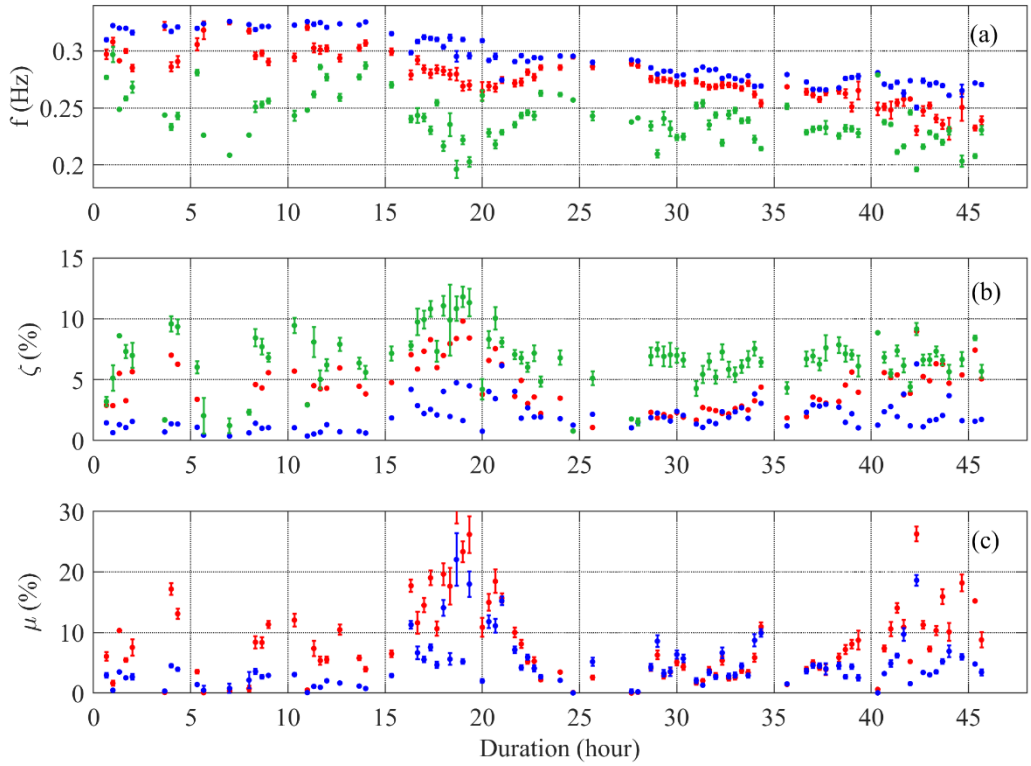

Figure 9 Tracking results of (a) natural frequencies, (b) damping ratios and (c) mass ratios. Red for Mode 1, blue for Mode 2 and green for TMD.

7 Conclusions

This work has proposed a Bayesian approach to identify the modal parameters of TMD and primary structure using ambient vibration data measured on the primary structure only. To highlight the contributions, the likelihood function and PSD matrix of data have been formulated (Sections 3.1 and 3.2). These have accounted for the inevitable non-classically damped modal dynamics in the combined structure-TMD system, although the primary structure is still assumed to be classically damped. Theoretical considerations have been made to come up with a consolidated set of parameters so that the Bayesian inference problem is globally identifiable (Section 3.3). Niche computational methodologies have also been developed for efficient calculation of Bayesian statistics, i.e., the posterior MPV by EM algorithm (Section 4.1) and analytical formulae for covariance matrix (Section 4.2). The proposed theory and computational algorithms have been verified using synthetic data (Section 5) and applied to field data (Section 6).

The frequency response function of the structure-TMD system has different characteristic behaviours, which depend on modal parameters (Section 2). This in turn affects the precision of the identification results. For example, the identification uncertainty (in terms of c.o.v.) generally increases with TMD damping ratio. When TMD damping ratio is large, the singular value spectrum of data is similar to the one without TMD. Such data may not carry enough information for distinguishing the TMD characteristics from those of the primary structure, lowering the sensitivity of parameters in the likelihood function and making parameter identification more challenging. The proposed theory does not require detailed information about the installation/orientation of TMD; related parameters are identified in the method.

Simplification in the problem parameterisation, referred as ‘independent tuning’, has been made to improve identifiability (Section 3.3). In reality, the ‘independent tuning’ assumption need not hold, and it is often not amendable/relevant for mathematical verification. Potential bias (when the assumption is violated) in the identification results has been investigated numerically, and is found to be acceptable. Thus, the assumption is believed to play a balance between tractability of the problem and approximation of reality. This is especially so when one considers other sources of uncertainty in field tests.

The proposed method is applicable whenever there is only one TMD taking action in the selected frequency band of the mode(s) of interest. E.g., it is applicable to a structure with two TMDs, each tuning a different mode on two different bands. This is because the method

operates in the frequency domain and it uses the FFT in the selected band only, and so modes or TMD action in other excluded bands do not appear in the likelihood function and hence need not be considered. This case is typical in applications. For the more general (though less common) case where there are multiple TMDs actions on the same mode(s) in the same band, extending the formulation or algorithm may not be easy. In particular, having multiple TMDs in the same band means there will be more parameters of similar nature, and they may not be identifiable, i.e., data may not contain adequate information to distinguish them.

8 Acknowledgements

This work is funded by the UK Engineering & Physical Sciences Research Council (Grant EP/N017897/1). The first author is supported by a tuition fellowship by the School of Engineering at the University of Liverpool, the second author by the Joint University of Liverpool/China Scholarship Council Scholarship, and the third author by grant SUG/4(C120032000) at Nanyang Technological University, Singapore. These financial supports are gratefully acknowledged. The authors would like to thank Prof. James Brownjohn at the University of Exeter for providing the chimney field data.

Appendix A. Initial guess for TMD parameters

This section presents some analytical results relating the TMD parameters to some simple features of the PSD of an undamped SDOF structure ($\zeta_1 = 0$). This forms the basis for the choice of initial guess in Section 4.1. We first present a discussion that leads to an initial guess for ω_d, ω_1 (and hence f_d, f_1), and μ. The initial guess for ζ_d requires more works and is presented in Appendix A.2 later.

A.1 Initial guess for ω_d, ω_1 and μ

In this section, we develop the initial guess for ω_d, ω_1 and μ by using the information related to the peaks and trough in the SV spectrum. Consider the structure-TMD system in Figure 1 but the primary structure is now assumed to be undamped. Substituting $\zeta_1 = 0$ into (9), the dynamic amplification reduces to

$$D = \frac{(1-\alpha^2\beta^2)^2 + (2\zeta_d\alpha\beta)^2}{[(1+\mu-\beta^2)(1-\alpha^2\beta^2)-\mu]^2 + (2\zeta_d\alpha\beta)^2(1+\mu-\beta^2)^2} \qquad (\zeta_1 = 0) \qquad (33)$$

When $\zeta_d = 0$, it is clear that D has a minimum of 0 when $\beta^2 = 1/\alpha^2$, i.e., when $\omega = \omega_d$. Also, D tends to infinity at the natural frequencies $\{\tilde{\omega}_i\}_{i=1}^2$ of the combined structure-TMD system because they zero the bracketed term in the denominator in (33); see (41) later. For non-zero but small ζ_d, D has a minimum near $\omega = \omega_d$ and two maxima near $\{\tilde{\omega}_i\}_{i=1}^2$. This suggests taking the trough location as an estimate for ω_d and the peak locations for $\{\tilde{\omega}_i\}_{i=1}^2$.

Note that $\{\tilde{\omega}_i\}_{i=1}^2$ and ω_d can be estimated from the SV spectrum. We next obtain an expression for ω_1 in terms of them to obtain an initial guess. Recall that the stiffness and mass matrices of the combined system are given by

$$\mathbf{K} = \begin{bmatrix} k_1 + k_d & -k_d \\ -k_d & k_d \end{bmatrix} = m \begin{bmatrix} \omega_1^2 + \mu\omega_d^2 & -\mu\omega_d^2 \\ -\mu\omega_d^2 & \mu\omega_d^2 \end{bmatrix} \qquad \mathbf{M} = \begin{bmatrix} m & \\ & m_d \end{bmatrix} = m \begin{bmatrix} 1 & \\ & \mu \end{bmatrix} \tag{34}$$

The characteristic equation $|\mathbf{K} - \lambda\mathbf{M}| = 0$ for $\lambda = \omega^2$ gives (after cancelling out m and m_d) a quadratic equation

$$\lambda^2 + B\lambda + C = 0 \qquad B = -[\omega_1^2 + (1+\mu)\omega_d^2] \qquad C = \omega_1^2\omega_d^2 \tag{35}$$

From the elementary property of the roots of quadratic equation, $\lambda_1 + \lambda_2 = -B$ and $\lambda_1\lambda_2 = C$, i.e.,

$$\tilde{\omega}_1^2 + \tilde{\omega}_2^2 = \omega_1^2 + (1+\mu)\omega_d^2 \tag{36}$$

$$\tilde{\omega}_1^2\tilde{\omega}_2^2 = \omega_1^2\omega_d^2 \tag{37}$$

The initial guess for ω_1 can be obtained by rearranging (37)

$$\omega_1 = \frac{\tilde{\omega}_1\tilde{\omega}_2}{\omega_d} \tag{38}$$

Replacing $\{\tilde{\omega}_i\}_{i=1}^2$ by peak locations and ω_d by trough location picked from SV spectrum and ω_1 from (38), rearranging (36) gives

$$\mu = \frac{\tilde{\omega}_1^2 + \tilde{\omega}_2^2 - (\omega_1^2 + \omega_d^2)}{\omega_d^2} = \frac{(\tilde{\omega}_1 - \tilde{\omega}_2)^2}{\omega_d^2} - \frac{(\omega_1 - \omega_d)^2}{\omega_d^2} \tag{39}$$

Since $|\tilde{\omega}_1 - \tilde{\omega}_2| \geq |\omega_1 - \omega_d|$, the initial guess of $\mu \approx [(\tilde{\omega}_1 - \tilde{\omega}_2)^2 - (\omega_1 - \omega_d)^2]/\omega_d^2$ is guaranteed to be non-negative.

Note that in terms of frequency ratio $\beta = \omega_1 / \omega$ the characteristic equation in (35) reads

$$1 + B\beta^2 + C\beta^4 = 0 \qquad B = -[1 + (1+\mu)\alpha^2] \qquad C = \alpha^2 \tag{40}$$

Substituting B and C gives $\alpha^2\beta^4 - [1 + (1+\mu)\alpha^2]\beta^2 + 1 = 0$, which can be rewritten as

$$(1 + \mu - \beta^2)(1 - \alpha^2\beta^2) - \mu = 0 \tag{41}$$

A.2 Initial guess for ζ_d

In this section, we develop an initial guess for ζ_d based on the trough/peak ratio of the SV spectrum. It is based on $\zeta_1 = 0$ and takes the trough and peaks as proxies for the points at $\omega = \omega_d$ (i.e., $\beta = 1/\alpha$) and $\tilde{\omega}_i$, respectively.

Substituting $\beta = 1/\alpha$ (proxy for trough location) into (33) gives

$$D = \frac{(2\zeta_d)^2}{\mu^2 + (2\zeta_d)^2(1 + \mu - 1/\alpha^2)^2} \qquad \left(\zeta_1 = 0, \quad \beta = \frac{1}{\alpha}\right) \tag{42}$$

Substituting $\tilde{\beta} = \omega_1 / \tilde{\omega}_i$ (proxy for peak locations) into (33) gives

$$D = \frac{(1 - \alpha^2\tilde{\beta}^2)^2 + (2\zeta_d\alpha\tilde{\beta})^2}{(2\zeta_d\alpha\tilde{\beta})^2(1 + \mu - \tilde{\beta}^2)^2} \qquad \left(\zeta_1 = 0, \quad \tilde{\beta} = \omega_1 / \tilde{\omega}_i\right) \tag{43}$$

Although the unknown modal force PSD appears as a multiplier in the SV spectrum, when the signal-to-noise (s/n) ratio is high, it is cancelled out in the ratio of the trough to peaks. Let such ratio be r. Then

$$\frac{\text{trough}}{\text{peak}} \approx \frac{D(\beta = 1/\alpha)}{D(\beta = \tilde{\beta})} = \frac{(2\zeta_d)^2}{\mu^2 + (2\zeta_d)^2(1 + \mu - 1/\alpha^2)^2} \times \frac{(2\zeta_d\alpha\tilde{\beta})^2(1 + \mu - \tilde{\beta}^2)^2}{(1 - \alpha^2\tilde{\beta}^2)^2 + (2\zeta_d\alpha\tilde{\beta})^2} \tag{44}$$

Setting this ratio to r and rearranging gives a quadratic equation $Ax^2 + Bx + C = 0$ for the variable $x = (2\zeta_d)^2$ where

$$\begin{aligned} A &= \alpha^2\tilde{\beta}^2[(1 + \mu - \tilde{\beta}^2)^2 - r(1 + \mu - 1/\alpha^2)^2] \\ B &= -r[(1 - \alpha^2\tilde{\beta}^2)^2(1 + \mu - 1/\alpha^2)^2 + \mu^2\alpha^2\tilde{\beta}^2] \\ C &= -r\mu^2(1 - \alpha^2\tilde{\beta}^2)^2 \end{aligned} \tag{45}$$

The initial guess for ζ_d is obtained from the larger root of the quadratic equation:

$$\zeta_d \approx \frac{1}{2}\sqrt{\frac{-B+\sqrt{\Delta}}{2A}} \qquad \Delta = B^2 - 4AC \tag{46}$$

The following analysis suggests that (46) gives a proper initial guess for ζ_d when $\mu > 0$ and $0 < r < 1$. First note that $\Delta \geq 0$ because, substituting A, B and C from (45) and simplifying,

$$\Delta = r^2[(1-\alpha^2\tilde{\beta}^2)^2(1+\mu-1/\alpha^2)^2 - \mu^2\alpha^2\tilde{\beta}^2]^2 + 4r\mu^2\alpha^2\tilde{\beta}^2(1-\alpha^2\tilde{\beta}^2)^2(1+\mu-\tilde{\beta}^2)^2 \tag{47}$$

which is always positive for $r > 0$ and $\mu > 0$. Thus, there are always two real roots of x. From (45), it is clear that $B < 0$ and $C \leq 0$. By noting that the sum of roots is $-B/A$ and the product of roots is C/A (or, more directly, using Routh-Hurwitz criterion), it can be shown that there is exactly one positive root of x (hence the legitimate value of ζ_d) if and only if $A > 0$. To investigate the latter possibility, note that $\tilde{\omega}_1 < \omega_d < \tilde{\omega}_2$. Dividing by ω_1 and taking reciprocals, this implies $\tilde{\beta}_1 > 1/\alpha > \tilde{\beta}_2$ and hence

$$.1+\mu-\tilde{\beta}_1^2 < 1+\mu-\frac{1}{\alpha^2} < 1+\mu-\tilde{\beta}_2^2. \tag{48}$$

There is then at least one $\tilde{\beta}_i$ such that $(1+\mu-\tilde{\beta}_i^2)^2 > (1+\mu-1/\alpha^2)^2$, making $A > 0$ for $0 < r < 1$ and hence returning a proper value for ζ_d from (46).

In (48), if the lower and upper bounds are of the same sign then $A > 0$ at only one $\tilde{\beta}_i$, i.e., $\tilde{\beta}_2$ when both bounds are positive and $\tilde{\beta}_1$ when negative. The following shows that the bounds are of opposite sign and hence it is possible for $A > 0$ at either $\tilde{\beta}_1$ or $\tilde{\beta}_2$, or both:

$$(1+\mu-\tilde{\beta}_1^2)(1+\mu-\tilde{\beta}_2^2) = (1+\mu)^2 + \tilde{\beta}_1^2\tilde{\beta}_2^2 - (1+\mu)(\tilde{\beta}_1^2+\tilde{\beta}_2^2) = -\frac{\mu}{\alpha^2} < 0 \tag{49}$$

after substituting $\tilde{\beta}_1^2 + \tilde{\beta}_2^2 = 1+\mu+1/\alpha^2$ and $\tilde{\beta}_1^2\tilde{\beta}_2^2 = 1/\alpha^2$ using the sum and product of the characteristic equation in (41).

As a remark, at the $\tilde{\beta}_i$ point where $A > 0$, one has $\Delta = 0$ if and only if $r = 0$; and so we always have $\Delta > 0$ if $r > 0$. To see this, substituting $r = 0$ gives $B = C = 0$ and hence $\Delta = 0$. Conversely, using (47) with $\Delta = 0$ implies $1-\alpha^2\tilde{\beta}^2 = 0$ (since $1+\mu-\tilde{\beta}^2 \neq 0$ when $A > 0$) and hence $C = 0$ and consequently $B^2 = 4AC = 0$ as well. From (45) this implies $r = 0$

because $\mu \neq 0$. Since $B = C = 0$ when $r = 0$ (or equivalently $\Delta = 0$), we have coincidentally $\zeta_d = 0$.

The above analysis assumes that $\zeta_1 = 0$. In implementation, the trough location is taken as a proxy for $\beta = 1/\alpha$, and the peak locations are taken as proxy for $\tilde{\beta}_i$. The quality of this approximation tends to deteriorate for non-zero ζ_1 or large ζ_d, where the peaks and troughs are less distinctive and r is closer to 1. For this reason, it is recommended to take $\tilde{\beta}_i$ as the point with smaller r.

Appendix B. Response RMS and equivalent damping

This section provides a method for evaluating the equivalent damping ratio based on TMD dynamics for SDOF structure. Assuming that the excitation *w* is stochastic stationary with PSD S_w (one-sided in $(N/kg)^2/Hz$), the displacement variance is given by [18]

$$\sigma_x^2 = \frac{S_w}{8\omega_1^3}\frac{P}{Q} \tag{50}$$

where

$$P = \mu\alpha^2(\alpha\zeta_1 + \zeta_d) + [1-(1+\mu)\alpha^2]^2\zeta_d + 4\alpha\zeta_d[\zeta_1 + (1+\mu)\alpha\zeta_d](\alpha\zeta_1 + \zeta_d) \tag{51}$$

$$Q = \mu\alpha(\alpha\zeta_1 + \zeta_d)^2 + [1-(1+\mu)\alpha^2]^2\zeta_1\zeta_d + 4\alpha\zeta_1\zeta_d\left[\zeta_1 + (1+\mu)\alpha\zeta_d\right](\alpha\zeta_1 + \zeta_d) \tag{52}$$

Check that when $\mu = 0$, $P/Q = 1/\zeta_1$ and so (50) reduces to the familiar SDOF variance formula.

In practice, the damping of a mode tuned by TMD may be empirically quantified by an equivalent damping ratio, which is defined so that the classical formula $S_w/8\omega_1^3\zeta_e$ returns the response variance with TMD. This gives

$$\zeta_e = \frac{S_w}{8\omega_1^3\sigma_x^2} = \frac{Q}{P} \tag{53}$$

When the parameters α , μ , ζ_1 and ζ_d are known (e.g., identified values), they can be substituted into P and Q to obtain ζ_e. Alternatively, with less specific reference to the structure-TMD modelling, one can assess ζ_e more directly from the knowledge of ω_1, S_w and

response variance. It is noted that vibration is often measured in terms of acceleration rather than displacement in the field setting. In this case, a simple approximation for the contribution due to a narrow resonance band is to take $\sigma_x^2 = \sigma_{\ddot{x}}^2 / \omega_1^4$, which gives

$$\zeta_e \approx S_w \omega_1 / 8\sigma_{\ddot{x}}^2 \tag{54}$$

Appendix C. Derivative calculations

This section provides the derivatives of $\mathbf{H}_k$ and modal FRF *g*, which are used to calculate the identification uncertainty. Their derivatives are respectively summarised in Tables 4 and 5, where the superscripted symbol $'^{(x)}$ and $'^{xy}$ denote the derivatives with respect to the corresponding variables.

Table 4 Derivatives of $g=[1-\beta^2+\mu(1-h_d)-2\zeta_1\beta\mathbf{i}]^{-1}$ for acceleration data.

$g^{(xy)}$		$y=$			
		β	ζ_1	μ	β_d,ζ_d
$x=$	β	$2(3\beta^2+1-4\zeta_1^2+6\mathbf{i}\zeta_1\beta+\mu(1-h_d))g^3$	$2\mathbf{i}(3\beta^2+1+2\mathbf{i}\zeta_1\beta+\mu(1-h_d))g^3$	$4(h_d-1)(\beta+\mathbf{i}\zeta_1)g^3$	$4\mu(\beta+\mathbf{i}\zeta_1)g^3h_d^{(y)}$
	ζ_1		$-8\beta^2g^3$	$4\mathbf{i}\beta(h_d-1)g^3$	$4\mathbf{i}\beta\mu g^3h_d^{(y)}$
	μ			$2(h_d-1)^2g^3$	$(1-\beta^2-\mu(1-h_d)-2\zeta_1\beta\mathbf{i})g^3h_d^{(y)}$
	β_d ζ_d	Sym.			$\mu h_d^{(xy)}g^2+2\mu^2g^3h_d^{(x)}h_d^{(y)}$
$g^{(y)}$		$2(\beta+\mathbf{i}\zeta_1)g^2$	$2\mathbf{i}\beta g^2$	$(h_d-1)g^2$	$\mu g^2h_d^{(y)}$

See Table 13.4 in [33] for the derivatives of h_d; replace β by β_d; replace ζ by ζ_d.

Table 5 Derivatives of $\mathbf{H}_k = \mathbf{g}_k \mathbf{S} \mathbf{g}_k^*$.

$\mathbf{H}_k^{(xy)}$		$y =$			
		f_j, ζ_j, μ_j	f_d, ζ_d	S_{jj}	U_{rs}, V_{rs}
$x =$	f_i ζ_i μ_i	$\left[S_{ij} g_{ik}^{(x)} g_{jk}^{(y)*} \mathbf{e}_{ij} + \delta_{ij} g_{ik}^{(xy)*} \mathbf{g}_k \mathbf{S} \mathbf{e}_{ii} \right]$ $+(\cdot)^*$	$\left[g_{ik}^{(xy)} \mathbf{e}_{ii} \mathbf{S} \mathbf{g}_k^* + g_{ik}^{(x)} \mathbf{g}_k^{(y)} \mathbf{S} \mathbf{e}_{ii} \right]$ $+(\cdot)^*$	$\delta_{ij} g_{ik}^{(x)} g_{ik}^* \mathbf{e}_{ii}$ $+(.)^*$	$\begin{cases} c\ g_{ik}^{(x)} g_{sk}^* \mathbf{e}_{rs} + (\cdot)^* & i = r \\ c\ g_{ik}^{(x)*} g_{rk} \mathbf{e}_{rs} + (\cdot)^* & i = s \end{cases}$ $c = 1$ for ; $c = \mathbf{i}$ for V_{rs}
	f_d ζ_d		$\left[\mathbf{g}_k^{(xy)} \mathbf{S} \mathbf{g}_k^* + \mathbf{g}_k^{(y)} \mathbf{S} \mathbf{g}_k^{(x)*} \right]$ $+(\cdot)^*$	$g_{jk}^{(x)} g_{jk}^* \mathbf{e}_{jj}$ $+(.)$	$c\ (g_{rk}^{(x)} g_{sk}^* + g_{rk} g_{sk}^{(x)*}) \mathbf{e}_{rs} + (\cdot)^*$ $c = 1$ for U_{rs} ; $c = \mathbf{i}$ for V_{rs}
	S_{ii}			**0**	**0**
	U_{ij} V_{ij}	Sym.			**0**
$\mathbf{H}_k^{(y)}$		$g_{jk}^{(y)*} \mathbf{g}_k \mathbf{S} \mathbf{e}_{jj} + (\cdot)^*$	$\mathbf{g}_k^{(y)} \mathbf{S} \mathbf{g}_k^* + (\cdot)^*$	$g_{jk} g_{jk}^* \mathbf{e}_{jj}$	$c g_{rk} g_{sk}^* \mathbf{e}_{rs} + (\cdot)^*$ $c = 1$ for U_{rs} ; $c = \mathbf{i}$ for V_{rs}

See Table 4 for the derivatives of g ; $(\cdot)^*$ denotes a term equal to the complex conjugate of the previous one.

References

[1] T.T. Soong, G.F. Dargush, Passive energy dissipation systems in structural engineering, Wiley, 1997.

[2] J. Connor, S. Laflamme, Structural motion engineering, Springer, 2014.

[3] K.C.S. Kwok, B. Samali, Performance of tuned mass dampers under wind loads, Eng. Struct. 17 (1995) 655–667.

[4] A. Kareem, T. Kijewski, Y. Tamura, Mitigation of motions of tall buildings with specific examples of recent applications, Wind Struct. 2 (1999) 201–251.

[5] A.K. Ghorbani-Tanha, A. Noorzad, M. Rahimian, Mitigation of wind-induced motion of Milad Tower by tuned mass damper, Struct. Des. Tall Spec. Build. 18 (2009) 371–385.

[6] A.Y. Tuan, G.Q. Shang, Vibration control in a 101-storey building using a tuned mass damper, J. Appl. Sci. Eng. 17 (2014) 141–156.

[7] X. Lu, Q. Zhang, D. Weng, Z. Zhou, S. Wang, S.A. Mahin, S. Ding, F. Qian, Improving performance of a super tall building using a new eddy-current tuned mass damper, Struct. Control Heal. Monit. 24 (2017) e1882.

[8] A. Larsena, E. Svensson, H. Andersen, Design aspects of tuned mass dampers for the Great Belt East Bridge approach spans, J. Wind Eng. Ind. Aerodyn. 54 (1995) 413–426.

[9] R.C. Battista, M.S. Pfeil, Reduction of vortex-induced oscillations of Rio–Niterói bridge by dynamic control devices, J. Wind Eng. Ind. Aerodyn. 84 (2000) 273–288.

[10] Y. Fujino, Y. Yoshida, Wind-induced vibration and control of Trans-Tokyo Bay crossing bridge, J. Struct. Eng. 128 (2002) 1012–1025.

[11] C.P. Deavy, A. Allsop, K. Jones, The Spire of Dublin, Struct. Eng. 83 (2005) 20–25.

[12] J.M.W. Brownjohn, E.P. Carden, C.R. Goddard, G. Oudin, Real-time performance monitoring of tuned mass damper system for a 183 m reinforced concrete chimney, J. Wind Eng. Ind. Aerodyn. 98 (2010) 169–179.

[13] P. Górski, Investigation of dynamic characteristics of tall industrial chimney based on

GPS measurements using Random Decrement Method, Eng. Struct. 83 (2015) 30–49.

[14] J.P. Den Hartog, Mechanical vibrations, Courier Corporation, 1985.

[15] G.B. Warburton, Optimum absorber parameters for various combinations of response and excitation parameters, Earthq. Eng. Struct. Dyn. 10 (1982) 381–401.

[16] R. Rana, T.T. Soong, Parametric study and simplified design of tuned mass dampers, Eng. Struct. 20 (1998) 193–204.

[17] S. V Bakre, R.S. Jangid, Optimum parameters of tuned mass damper for damped main system, Struct. Control Heal. Monit. Off. J. Int. Assoc. Struct. Control Monit. Eur. Assoc. Control Struct. 14 (2007) 448–470.

[18] S. Krenk, J. Høgsberg, Tuned mass absorbers on damped structures under random load, Probabilistic Eng. Mech. 23 (2008) 408–415.

[19] S. Sgobba, G.C. Marano, Optimum design of linear tuned mass dampers for structures with nonlinear behaviour, Mech. Syst. Signal Process. 24 (2010) 1739–1755.

[20] S. Salcedo-Sanz, C. Camacho-Gómez, A. Magdaleno, E. Pereira, A. Lorenzana, Structures vibration control via tuned mass dampers using a co-evolution coral reefs optimization algorithm, J. Sound Vib. 393 (2017) 62–75.

[21] E. Reynders, System identification methods for (operational) modal analysis: review and comparison, Arch. Comput. Methods Eng. 19 (2012) 51–124.

[22] R. Brincker, C. Ventura, Introduction to operational modal analysis, John Wiley & Sons, 2015.

[23] M. Döhler, L. Mevel, Fast multi-order computation of system matrices in subspace-based system identification, Control Eng. Pract. 20 (2012) 882–894. https://doi.org/10.1016/j.conengprac.2012.05.005.

[24] B. Peeters, G. De Roeck, Stochastic System Identification for Operational Modal Analysis: A Review, J. Dyn. Syst. Meas. Control. 123 (2001) 659. https://doi.org/10.1115/1.1410370.

[25] B. Moaveni, E. Asgarieh, Deterministic-stochastic subspace identification method for identification of nonlinear structures as time-varying linear systems, Mech. Syst. Signal

Process. 31 (2012) 40–55.

[26] R. Brincker, L. Zhang, P. Andersen, Modal identification of output-only systems using frequency domain decomposition, Smart Mater. Struct. 10 (2001) 441–445. https://doi.org/10.1088/0964-1726/10/3/303.

[27] M. Döhler, L. Mevel, Efficient multi-order uncertainty computation for stochastic subspace identification, Mech. Syst. Signal Process. 38 (2013) 346–366.

[28] E. Reynders, K. Maes, G. Lombaert, G. De Roeck, Uncertainty quantification in operational modal analysis with stochastic subspace identification: Validation and applications, Mech. Syst. Signal Process. 66 (2016) 13–30.

[29] S. Greś, M. Döhler, L. Mevel, Uncertainty quantification of the Modal Assurance Criterion in operational modal analysis, Mech. Syst. Signal Process. 152 (2021) 107457.

[30] P. Mellinger, M. Döhler, L. Mevel, Variance estimation of modal parameters from output-only and input/output subspace-based system identification, J. Sound Vib. 379 (2016) 1–27.

[31] J.L. Beck, Bayesian system identification based on probability logic, Struct. Control Heal. Monit. 17 (2010) 825–847.

[32] K. Yuen, L.S. Katafygiotis, Bayesian time - domain approach for modal updating using ambient data, 16 (2001). https://doi.org/10.1260/136943303769013183.

[33] S.-K. Au, Operational Modal Analysis: Modeling, Bayesian Inference, Uncertainty Laws, Springer, 2017.

[34] J.L. Beck, L.S. Katafygiotis, Updating models and their uncertainties. I: Bayesian statistical framework, J. Eng. Mech. 124 (1998) 455–461.

[35] B. Weber, G. Feltrin, Assessment of long-term behavior of tuned mass dampers by system identification, Eng. Struct. 32 (2010) 3670–3682.

[36] J.M.W. Brownjohn, E.P. Carden, C.R. Goddard, G. Oudin, Real-time performance monitoring of tuned mass damper system for a 183 m reinforced concrete chimney, J. Wind Eng. Ind. Aerodyn. 98 (2010) 169–179. https://doi.org/10.1016/j.jweia.2009.10.013.

[37] A.J. Roffel, R. Lourenco, S. Narasimhan, S. Yarusevych, Adaptive compensation for detuning in pendulum tuned mass dampers, J. Struct. Eng. 137 (2011) 242–251.

[38] J.-F. Wang, C.-C. Lin, Extracting parameters of TMD and primary structure from the combined system responses, Smart Struct. Syst. 16 (2015) 937–960.

[39] B. Hazra, A. Sadhu, R. Lourenco, S. Narasimhan, Re-tuning tuned mass dampers using ambient vibration measurements, Smart Mater. Struct. 19 (2010) 115002.

[40] A. Sadhu, B. Hazraa, S. Narasimhan, Ambient modal identification of structures equipped with tuned mass dampers using parallel factor blind source separation, Smart Struct. Syst. 13 (2014) 257–280.

[41] M. Yuan, A. Sadhu, K. Liu, Condition assessment of structure with tuned mass damper using empirical wavelet transform, J. Vib. Control. 24 (2018) 4850–4867.

[42] Z. Cao, X. Hua, Q. Wen, Z. Chen, H. Niu, A state space technique for modal identification of coupled structure–tuned mass damper systems from vibration measurement, Adv. Struct. Eng. 22 (2019) 2048–2060.

[43] T.K. Caughey, M.E. O'Kelly, Classical normal modes in damped linear dynamic systems, (1965).

[44] S. Adhikari, Damping modelling using generalized proportional damping, J. Sound Vib. 293 (2006) 156–170. https://doi.org/10.1016/j.jsv.2005.09.034.

[45] B. Li, S.-K. Au, An expectation-maximization algorithm for Bayesian operational modal analysis with multiple (possibly close) modes, Mech. Syst. Signal Process. 132 (2019) 490–511.

[46] Z. Zhu, S.-K. Au, B. Li, Y.-L. Xie, Bayesian operational modal analysis with multiple setups and multiple (possibly close) modes, Mech. Syst. Signal Process. 150 (2021) 107261.

[47] F.J. Cara, J. Carpio, J. Juan, E. Alarcón, An approach to operational modal analysis using the expectation maximization algorithm, Mech. Syst. Signal Process. 31 (2012) 109–129. https://doi.org/10.1016/j.ymssp.2012.04.004.

[48] M. El-Kafafy, T. De Troyer, P. Guillaume, Fast maximum-likelihood identification of

modal parameters with uncertainty intervals: a modal model formulation with enhanced residual term, Mech. Syst. Signal Process. 48 (2014) 49–66.

[49] T.J. Matarazzo, S.N. Pakzad, STRIDE for structural identification using expectation maximization: iterative output-only method for modal identification, J. Eng. Mech. 142 (2016) 4015109.

[50] A.P. Dempster, N.M. Laird, D.B. Rubin, Maximum likelihood from incomplete data via the EM algorithm, J. R. Stat. Soc. Ser. B. 39 (1977) 1–22.

[51] J.B. Elsner, A.A. Tsonis, Singular spectrum analysis: a new tool in time series analysis, Springer Science & Business Media, 1996.

[52] A. Zhigljavsky, Singular spectrum analysis for time series: Introduction to this special issue, Stat. Interface. 3 (2010) 255–258.

[53] S.-K. Au, Connecting Bayesian and frequentist quantification of parameter uncertainty in system identification, Mech. Syst. Signal Process. 29 (2012) 328–342.

[54] S.-K. Au, J.M.W. Brownjohn, B. Li, A. Raby, Understanding and managing identification uncertainty of close modes in operational modal analysis, Mech. Syst. Signal Process. 147 (2021) 107018.

[55] J.K. Galsworthy, B.J. Vickery, Wind loads and interference effects for new and existing chimneys at the Rugeley power station, UK, Alan Davenport Wind Eng. Group, Bound. Layer Wind Tunn. Lab. London, Ontario, Canada, N6A 5BP. (2006).

[56] C.R. Goddard, The design of the 183m new chimney, Rugeley, UK-interference effects, CICIND, Esbjerg, Denmark. (2007).